

Otolith chemistry of *Electrona antarctica* suggests a potential population marker distinguishing the southern Kerguelen Plateau from the eastward-flowing Antarctic Circumpolar Current.

Mi Duan^{1,2,3}, Julian R. Ashford⁴, Sophie Bestley⁵, Xiaoying Wei^{1,2,3}, Andrea Walters⁵, Guoping Zhu^{1,2,3,6,*}

¹ College of Marine Sciences, Shanghai Ocean University, Shanghai 201306, China

² Center for Polar Research, Shanghai Ocean University, Shanghai 201306, China

³ Polar Marine Ecosystem Group, The Key Laboratory of Sustainable Exploitation of Oceanic Fisheries Resources, Ministry of Education, Shanghai 201306, China

⁴ Center for Quantitative Fisheries Ecology, Old Dominion University, 800 West 46th St., Norfolk, VA 23529, USA

⁵ Institute for Marine and Antarctic Studies, University of Tasmania, Private Bag 129, Hobart TAS 7001, Australia

⁶ National Engineering Research Center for Oceanic Fisheries, Shanghai 201306, China

* Corresponding author: gpzhu@shou.edu.cn

Abstract: Large submarine plateaus impede the eastward flow of the deep-reaching Antarctic Circumpolar Current (ACC), and at the southern Kerguelen Plateau (SKP), the ACC flow is steered north through the Fawn Trough and south through the Princess Elizabeth Trough. During the Kerguelen Axis study (K-AXIS), a regional-scale ecosystem survey, oceanographic sampling showed the ACC water properties west of the SKP to be distinct from those over the SKP. *Electrona antarctica*, a dominant mesopelagic fish species, is associated with Circumpolar Deep Water transported by the ACC, and modified versions that occur over and downstream from the SKP including along the Antarctic continental slope. Here, otolith chemistry from samples of *E. antarctica* collected during K-AXIS were used to test a biophysical hypothesis predicting structuring and movement between populations along zonal flow in the ACC. In chemistry deposited during early life in the otolith nuclei, the relationship between $MgCa^{-1}$ and $SrCa^{-1}$ showed complete separation between fish collected over the SKP and within the ACC proper, indicating population differentiation. Chemistry from the otolith edges, deposited during the period leading up to capture, showed significantly higher concentrations of $MgCa^{-1}$ over the SKP, likely related to differences in feeding and reproduction. Fish with nucleus chemistry characteristic of the SKP were also found in samples caught further east, suggesting they were transported along the ACC downstream, and southward towards the Antarctic continent within the Australian–Antarctic Gyre.

Keywords: *Electrona antarctica*; otolith chemistry; Antarctic Circumpolar Current; Fawn Trough Current; Circumpolar Deep Water; water mass; residency.

Introduction

Antarctic lanternfishes (*Electrona antarctica* Günther 1978) are the most abundant mesopelagic fish found south of the Antarctic Polar Front in the Southern Ocean, with a circumpolar distribution (Figure 1) that extends into the high Antarctic along the Antarctic Slope Front (Andriashev 1965; Collins et al. 2012; Duhamel et al. 2014). Occupying an important trophic role in the transfer of energy through Southern Ocean food webs (Van de Putte et al. 2010), these fish are predators on mesozooplankton (Hureau 1994; Clarke et al. 2018; Riaz et al. 2019) and their high lipid content (Lea et al. 2002) makes them important energy-rich prey for marine predators, including penguins and seals (Ainley et al. 1986; Loots et al. 2007). Extensive diel vertical migrations, which span the water column from the upper 50 m during the night to 400 m and deeper during the day (Hulley and Duhamel 2011), help export carbon to the mesopelagic layers (Pakhomov et al. 1996) contributing to biogeochemical cycling within the Southern Ocean.

The Southern Ocean is characterized by strong zonal wind stress, which drives eastward flow in the Antarctic Circumpolar Current (hereafter, the Current). The classical view of the Current transport is that it is concentrated along three main circumpolar fronts (the Sub-Antarctic Front, Polar Front and Southern Antarctic Circumpolar Current Front), in jets with velocities up to 0.5 ms^{-1} (e.g., Orsi et al. 1995) capable of circulating water around the Antarctic on time scales of 3 - 5 years.

More recently, hydrographical, satellite-based and high-resolution modelling studies have demonstrated that the major fronts of the Current consist of multiple dynamic branches (see Sokolov and Rintoul 2009a; Rintoul 2018). The Current carries warm nutrient-rich Circumpolar Deep Water around the Southern Ocean. The saline lower limb of Circumpolar Deep Water is dense enough to penetrate into the subpolar zone south of the Current, largely remaining below any direct surface influence. However, in the Ross Sea, intrusions over the deep shelf mix with overlying Antarctic Surface Water to form a modified version (e.g. Orsi and Wiederwohl 2009). The upper limb of Circumpolar Deep Water, characterized by low oxygen, shoals poleward across the Current as part of the meridional overturning circulation, and the Southern Boundary of the Current marks its southernmost extent (Orsi et al. 1995). Off East Antarctica, as the upper limb of Circumpolar Deep Water shoals its properties are transformed through mixing with overlying Antarctic Surface Water and by air-sea and sea-ice interactions, and the altered water mass spreads south of the Southern Boundary of the Current as modified Circumpolar Deep Water (Bindoff et al. 2000; Meijers et al. 2010; Williams et al. 2010). Along the western Antarctic Peninsula, the Southern Antarctic Circumpolar Current Front is located over the continental slope and the upper limb of Circumpolar Deep Water can gain direct access over the Antarctic continental shelf where intrusions mix with the overlying Winter Water to form another version of the upper limb of Circumpolar Deep Water (e.g., Smith et al. 1999; Dinniman and Klinck 2004).

Associations between *E. antarctica* and oceanographic features have long been proposed (e.g., McGinnis 1982). Hulley and Duhamel (2011) linked abundance and distribution to Circumpolar Deep Water in the South Atlantic and the Kerguelen Plateau region. Off the western Antarctic Peninsula, Donnelly and Torres (2008) found the species distributed as part of an oceanic assemblage associated with unaltered Circumpolar Deep Water in the Current. They noted that overlap with a neritic assemblage inshore was related to intrusions of oceanic water and widespread coverage of modified Circumpolar Deep Water over the shelf. Similarly, Parker et al. (2015) found *E. antarctica* distribution over the south-western Antarctic Peninsula shelf corresponded to strong oceanic influence and the presence of modified Circumpolar Deep Water close inshore. Sampling along East Antarctica between 80° E near Prydz Bay and 150° E over the George V Shelf, Hoddell et al. (2000) reported that larvae contributed to an assemblage associated with cold ocean water north of the continental slope, whereas adults increased where a warm water mass indicated a southward turn in the Current. Off Wilkes Land (110-140° E), Moteki et al. (2017) reported *E. antarctica* larvae to be mainly distributed in modified Circumpolar Deep Water over the upper 200 m near the Southern Boundary. Larval assemblages have also been found at high latitudes in the Indian Ocean and Pacific Ocean sectors by Efremenko (1983); along East Antarctica in the Lazarev Sea (Flores et al. 2008; Van de Putte et al. 2010) and Lützow-Holm Bay (Moteki et al. 2009); near the Antarctic Peninsula off the South Shetland Islands (Kellermann and Kock 1988) and in the

Bransfield Strait (Kellermann and Schadwinkel 1991); across the Scotia Sea (Efremenko 1986); and around South Georgia (North 1987). Nevertheless, despite the importance of *E. antarctica* to the Southern Ocean system, its population structure remains poorly understood.

Recently, Zhu et al. (2018) used otolith chemistry to show clear differentiation between *E. antarctica* caught in eastward and westward transport pathways along the Southern Antarctic Circumpolar Current Front and the Antarctic Slope Front in the southern Kerguelen region. The chemical composition of fish otoliths is widely used to answer biological and ecological questions related to movement and habitat use (Izzo et al. 2018). Otoliths grow continuously throughout life, forming daily and annual growth bands composed of a calcium carbonate lattice that is not re-metabolized once deposited (Campana 1999). Trace and minor elements preferentially bind within the crystalline aragonite matrix laid down over the life history (Elsdon et al. 2008) and can be considered as natural markers (e.g., Patterson et al. 2005) that reflect environmental exposures.

In the Southern Ocean, the chemistry in material laid down along the otolith edge just prior to capture has empirically discriminated hydrographic features along the Current and the Antarctic continental shelf (Ashford et al. 2005, 2007, 2010, 2012a, 2012b). Otolith concentrations of MgCa^{-1} , SrCa^{-1} and BaCa^{-1} have revealed differences between environments influenced by the Circumpolar Deep Water and

other water masses; and different versions of the Circumpolar Deep Water. Although the underlying mechanisms of incorporation have yet to be fully described, differences in $BaCa^{-1}$ are thought to reflect ambient levels of dissolved Ba (Campana 1999, Ashford et al. 2005) whereas $MgCa^{-1}$ and $SrCa^{-1}$ are directly influenced by physiology. $SrCa^{-1}$ is considered to reflect growth mediated by ambient temperature and food availability (Campana 1999) and $MgCa^{-1}$ to reflect fish activity like reproduction and movement (Ashford et al. 2005; Zhu et al. 2018; Caccavo et al. 2019). Chemistry deposited during early life in otolith nuclei has been used to test population hypotheses in Patagonian toothfish (*Dissostichus eleginoides*) (Ashford et al. 2006, 2008, 2012a), Scotia Sea icefish (*Chaenocephalus aceratus*) (Ashford et al. 2010), Antarctic toothfish (*Dissostichu smawsoni*) (Ashford et al. 2012b), and Antarctic silverfish (*Pleuragramma antarcticum*) (Caccavo et al. 2019).

Zhu et al. (2018) proposed a biophysical hypothesis that predicted structuring between populations of *E. antarctica* along the Current based on regional retention mechanisms, with potentially extensive connectivity and mixing along zonal flow. In our study region, the southern Kerguelen Plateau presents a major barrier (Figure 2) and the zonal Current flow steers around the topography (Heywood et al. 1999; Park et al. 2009). Regional oceanographic properties show clear separation between the Current proper and water over the southern Kerguelen Plateau, which is quiescent with a slow anti-cyclonic circulation, high residence times and moderate productivity (Bestley et al. 2018; see Supporting information Figure S1 and accompanying

Supplement text for further details). The Current signature over the southern Kerguelen Plateau is moderated compared to signatures further west (Bestley et al. 2018) where the branches of the Southern Antarctic Circumpolar Current Front. Its northern branch of the Southern Antarctic Circumpolar Current Front steers around BANZARE Bank through the Fawn Trough together with the southern branch of the Polar Front (Sokolov and Rintoul 2009a, b; van Wijk et al. 2010); this intensified flow is deflected by the Chun Spur to turn south in the Fawn Trough Current. The southern branch of the Southern Antarctic Circumpolar Current Front and the Southern Boundary of the Current steer south of BANZARE Bank to pass jointly through the Princess Elizabeth Trough. These fronts turn sharply to the north in a dynamic deep Western Boundary Current (McCartney and Donohue 2007), then retroflect to the south and continue eastward with extensive meandering and both cyclonic and anticyclonic eddies. We tested for the structuring predicted by Zhu et al. (2018), by sampling fish from the hydrographically distinct regions over the southern Kerguelen Plateau and in the Current and comparing their otolith chemistry.

Materials and methods

Sample collection

Sampling was conducted during the Kerguelen Axis (K-AXIS) regional-scale marine ecosystem study focused on the southern Kerguelen Plateau (Figure 2).

Results from the oceanographic survey are published in Bestley et al. (2018). *E. antarctica* were captured from 4 to 14 February 2016 on board R.S.V. *Aurora Australis*, using the sampling methodology documented by Zhu et al. (2018). Samples were taken over the southern Kerguelen Plateau and from the Current waters (Table 1, Figure 2), corresponding to stations, where the conductivity-temperature-depth profiler (CTD) was deployed, along transects T6 and T9, designed to traverse key oceanographic transitions respectively along and across the axis of the southern Kerguelen Plateau. In the Antarctic Zone over the southern Kerguelen Plateau (AZ-SKP), fish were sampled at Stations 21, 22, and 23 along T6, where midwater opening/closing (MIDOC) multiple cod-end device net was deployed. Along T9, fish were sampled at Stations 34, 35, and 36 in the Antarctic Zone corresponding to the Current (AZ-ACC) further west, and at MIDOC Station 30 in the Antarctic Zone corresponding to Fawn Trough Current (AZ-FTC) to the east. After collection, standard length (SL) was measured to the nearest mm and fish were frozen at - 20 °C.

Potential temperature-salinity curves (Figure 3) along T9, with its vertical profile (Figure 4), show the structure of waters in the Current and over the southern Kerguelen Plateau. Shoaling isopycnals (Figure 4) between 80 ° E - 82 ° E (Stations 41 – 42) indicate a northerly flow (into the page) along the western flank of BANZARE Bank, whereas the strongly downward sloping isopycnals at 86 ° E (CTD Stations 38 - 39) are associated with the stronger southward flow (out of the page) of the Fawn Trough Current at the eastern plateau flank (Figure 4d). The temperature-

salinity and oxygen plots (Figure 3), together with vertical CTD profiles for the stations sampled for otolith chemistry (Supplement Figure 2), showed clear distinctions in the water properties to which fish were exposed during diel vertical migrations. At all stations excepting the Fawn Trough Current, a cold layer of Winter Water was found below the seasonal mixed layer within the Antarctic Surface Water at the near surface. In the AZ-ACC west of the southern Kerguelen Plateau, the Winter Water was located between 60 m – 100 m at Stations 42 and 44 and was slightly deeper and colder at Station 43 (60 m – 120 m, $-1.7\text{ }^{\circ}\text{C}$ versus $-0.9\text{ }^{\circ}\text{C}$ T_{min}). In the AZ-SKP at Stations 29-31, Winter Water was generally thicker and deeper (60 m – 140 m) and the temperature minimum somewhat colder ($> -1.1\text{ }^{\circ}\text{C}$). By contrast, water at the same depths was much warmer ($> 0.5\text{ }^{\circ}\text{C}$) at Station 38 in the AZ-FTC consistent with the influence of the Polar Front co-located with the northern branch of Southern Antarctic Circumpolar Current Front here. Below the Winter Water, the Circumpolar Deep Water in the AZ-SKP was more saline, had higher oxygen levels, and was colder at the same depths than the stations in the AZ-ACC further west. The corresponding depths at Station 38 in the AZ-FTC were consistently warmer than at the stations over the southern Kerguelen Plateau, and salinities were lower deeper than in either the AZ-SKP or AZ-ACC.

Samples of *E. antarctica* were also taken along T9 in the Western boundary Current at MIDOC Station 31, and along T6 in the Subpolar Zone south of the Southern Boundary at MIDOC Station 16 (Figure 2, Table 1). There, some of the

westward Antarctic Slope Current flow along the Antarctic continental slope turns offshore and feeds into the Southern Boundary and the Western Boundary Current (McCartney and Donohue 2007; Bindoff et al. 2000; Bestley et al. 2018), forming the western edge of the cyclonic Australia-Antarctic Gyre. At Station 39 in the Western Boundary Current, corresponding to MIDOC Station 31, Circumpolar Deep Water was colder at the same depths and showed higher oxygen levels than the AZ-SKP and AZ-ACC (Figure 3, Supporting information Figure S2), consistent with variable extension of subpolar waters from south of the Southern Boundary of the Current, and propagation of a cyclonic eddy northward along the Western Boundary Current (Bestley et al. 2018). At MIDOC Station 16, the water column was colder still (Supplement Figure 2), consistent with its position in the Australia-Antarctic Gyre south of the Southern Boundary of the Current and north of the Antarctic Slope Front.

Otolith processing

The otoliths were removed in the laboratory at the Australian Antarctic Division (AAD) and stored in plastic vials for later analysis. Otolith samples were transported to the laboratory at the College of Marine Sciences, Shanghai Ocean University (SHOU). Otoliths from a total of 36 fish were selected randomly. To remove any surface contamination, the otoliths were rinsed, sonicated for 5 min, then rinsed again, all in Milli-Q water, and left to dry. After drying, the weight (mg) of the otoliths was recorded using high precision scales (METTLER TOLEDO XPR2), and the right or

left otolith was randomly selected for processing. Otoliths were mounted individually on slides using crystal bond, which had been previously tested to ensure it was not a source of contamination, and ground from the posterior side to reveal a transverse plane through the otolith nucleus. Each whole otolith was embedded in crystal bond and dried for 24 - 48 h. The mounted otoliths were ground by hand using a grinder (REMET LS2) with 600 and 734 grit waterproof sandpaper, followed by 1200 and 2500 grit, until the nucleus was clearly exposed. Finally, the exposed surface was polished using 0.3 μm alumina powder, and age determined as described in Zhu et al. (2018, 2020) (Figure 5).

Trace element analysis

Otoliths were analysed using laser ablation inductively coupled plasma mass spectrometry (LA-ICP-MS) at the Wuhan SampleSolution Analytical Technology Co., Ltd., Wuhan, China. Detailed operating conditions for the laser ablation system and the ICP-MS instrument and data reduction can be found in Zong et al. (2010). Laser sampling was performed using a GeolasPro laser ablation system that consists of a COMPexPro 102 ArF excimer laser (wavelength of 193 nm and maximum energy of 200 mJ) and a MicroLas optical system. An Agilent 7900 ICP-MS instrument was used to acquire ion-signal intensities. Helium was applied as a carrier gas. Argon was used as the make-up gas and mixed with the carrier gas via a T-connector before entering the ICP. A “wire” signal smoothing device is included in

this laser ablation system (Hu et al. 2015). The spot size and frequency of the laser were set to 32 μm and 5 Hz, respectively. Trace element compositions of otoliths were calibrated against reference materials (BHVO-2G, BCR-2G and BIR-1G) without using an internal standard (Liu et al. 2008). Each analysis incorporated a background acquisition of approximately 20 - 30 s followed by 50 s of data acquisition from the sample; each reading consisted of 250 scans. An Excel-based software ICPMS DataCal was used to perform off-line selection and integration of background and analyzed signals, time-drift correction and quantitative calibration for trace element analysis (Liu et al. 2010). Otoliths were analysed for ^{42}Ca , ^{24}Mg , ^{55}Mn , ^{88}Sr , and ^{137}Ba and reported as ratios to ^{42}Ca . To calculate element:Ca (MeCa^{-1}) ratios, background counts were subtracted from otolith counts by interpolating between blank readings, and the corrected otolith counts were converted to MeCa^{-1} concentrations using the reference readings. To test for population heterogeneity, we sampled the nucleus, corresponding to early growth after hatching, using a spot raster. We also sampled the edge of the otolith corresponding to recent growth prior to capture.

Statistical analysis

Statistical analyses followed the approach established in Ashford et al. (2006; 2007; 2008, 2010, 2012b). For the main comparisons, edge and nucleus data ($n = 27$ for each) from the AZ-ACC, AZ-SKP and AZ-FTC were checked for relationships

with age and sex, and none were found. They were also checked for multivariate outliers by plotting robust squared Mahalanobis distances of the residuals (DI^2) against the corresponding quantiles (QQ plot) of the χ^2 distribution (Khattree and Naik 1999), and none were found. Univariate power transformations (e.g., Kuehl 1994) were used to stabilize the variances. The data transformations selected for the nucleus data were $y^{0.1}$ for $MgCa^{-1}$, $y^{0.8}$ for $SrCa^{-1}$ and $y^{0.5}$ for $BaCa^{-1}$. The same transformations were used for the edge data for $MgCa^{-1}$ and $BaCa^{-1}$; the distribution of $SrCa^{-1}$ showed a longer tail than in the nucleus data, and the transformation $y^{0.1}$ was used instead. The transformed data conformed to multivariate normality based on tests using Mardia's multivariate skewness ($p = 0.95$ for the nucleus data; $p = 0.54$ for the edge data) and kurtosis ($p = 0.18$ for the nucleus data; $p = 0.54$ for the edge data) measures, as well as QQ plots of squared Mahalanobis distances (di^2); variance-covariance matrices were equal according to Bartlett's modification ($p = 0.42$ for the nucleus data, and $p = 0.28$ for the edge data) (Khattree and Naik 1999).

Multivariate analysis of variance was used to test the nucleus data for population differences between fish caught over the southern Kerguelen Plateau at MIDOC Stations 21 - 23 (AZ-SKP_{nucleus}; $n = 14$), compared to fish caught in the Current at MIDOC Stations 34 - 36 and in the Fawn Trough Current at MIDOC Station 30 (AZ-ACC/FTC_{nucleus}; $n = 13$), and to test the corresponding edge data for differences in environmental exposure between the quiescent water over the southern Kerguelen Plateau (AZ-SKP_{edge}; $n = 14$) and the eastward-flowing Current including the Fawn

Trough Current (AZ-ACC/FTC_{edge}; n= 13). We found no evidence of any differences between fish from the AZ-ACC and AZ-FTC from the nucleus or edge data distributions; thus fish from these stations were pooled as representative of the Current. Univariate analyses were used to examine the contributions of each MeCa⁻¹; all data fulfilled univariate assumptions for normality (Kolmogorov Smirnov tests, at level $\alpha = 0.05$) and homoscedasticity (F_{\max} tests, at level $\alpha = 0.05$).

Since nucleus data for the southern Kerguelen Plateau and the Current fish showed complete separation, these were used as a training set in Multivariate Discriminant Analysis to define criteria for detecting fish with nucleus chemistry corresponding to the southern Kerguelen Plateau. The samples from the Western Boundary Current (MIDOC Station 31, n = 5), and the Australia-Antarctic Gyre (MIDOC Station 16, n = 4) were used as a test data set. The test data were transformed as for the training set, and Multivariate Discriminant Analysis was applied using a pooled covariance matrix (Khatree and Naik 2000) with equal prior probabilities of 50%, and error rates were estimated by cross-validation.

Results

The oceanographic survey clearly demonstrated that fish caught at MIDOC Stations 34 - 36 and MIDOC Station 30 occupied flow in the AZ-ACC/FTC, whereas those at MIDOC Stations 21 - 23 occupied the slow anti-cyclonic circulation

associated with the AZ-SKP. Moreover, the CTD data showed the clear distinctions in water properties to which fish were exposed during diel vertical migration. Ages for fish caught ranged from 2-6 years for the AZ-SKP and 2-7 years for the AZ-ACC/FTC (Table 2); 11 of 14 fish caught over the southern Kerguelen Plateau were 3 or 4 years old. Males and females were found in both regions, with a higher proportion of males over the southern Kerguelen Plateau. ^{24}Mg , ^{42}Ca , ^{88}Sr and ^{137}Ba used in this study showed concentrations that were well above the detection limits (Tables 3 and 4). In the chemistry deposited in the nuclei during early life (Figure 6a), the relationship between MgCa^{-1} and SrCa^{-1} showed clear separation between AZ-SKP and AZ-ACC/FTC fish, with higher levels of MgCa^{-1} over the southern Kerguelen Plateau consistent with strong population differentiation. The relationship between MgCa^{-1} and BaCa^{-1} also showed strong separation. In the chemistry deposited along the otolith edges prior to capture (Figure 6b), MgCa^{-1} was much higher for the AZ-SKP fish than the AZ-ACC/FTC. Notably, fish with edge concentrations of MgCa^{-1} higher than 49.0 ppm were all found at MIDOC Station 21 over the southern Kerguelen Plateau.

Using Multivariate analysis of variance to examine MgCa^{-1} , SrCa^{-1} and BaCa^{-1} at the nucleus, differences between AZ-SKP and AZ-ACC/FTC fish were highly significant (Pillai's Trace; $F_{3,23} = 25.35$; $p < 0.0001$). Differences in the univariate analyses were significant for MgCa^{-1} (ANOVA; $F = 27.22$; $p < 0.0001$), but not SrCa^{-1} (ANOVA; $F = 0.07$; $p = 0.79$) or BaCa^{-1} (ANOVA; $F = 0.10$; $p = 0.75$). The

Multivariate analysis of variance approach also identified significant differences between AZ-SKP and AZ-ACC/FTC fish in the edge chemistry (Pillai's Trace; $F_{3,23} = 6.89$; $p = 0.002$). Similar to the nucleus chemistry results, the univariate analyses identified significant differences for $MgCa^{-1}$ (ANOVA; $F = 13.3$; $p < 0.001$), but not $SrCa^{-1}$ (ANOVA; $F = 0.03$; $p = 0.866$) or $BaCa^{-1}$ (ANOVA; $F = 0.29$; $p = 0.595$).

For the cross-validation in the Multivariate Discriminant Analysis, all of the observations in the training set correctly classified to the AZ-SKP and AZ-ACC/FTC treatments (error-rate = 0%). In the test data (Table 5), four of the five fish taken in the Western Boundary Current allocated to the AZ-ACC/FTC (posterior probabilities between 70-100%) and one classified to the AZ-SKP (posterior probability of 100%). Two fish caught in the Australia-Antarctic Gyre also showed nucleus chemistry corresponding to the AZ-SKP, with posterior probabilities of 98% and 88% (Table 5, Fig. 7). The other two classified to the AZ-ACC/FTC with probabilities of 77% and 100%.

Discussion

Complete separation in nucleus chemistry suggests a population marker

Our results illustrate how otolith chemistry can help resolve spatially precise predictions from a population hypothesis, when undertaken in the context of the circulation and environment. By sampling in conjunction with an oceanographic survey, we were able to test predictions by Zhu et al. (2018) comparing fish that occupied a retention area over the southern Kerguelen Plateau and eastward-flowing water along the Current. The chemistry measured in the otolith nuclei separated completely along the relationship between $MgCa^{-1}$ and $SrCa^{-1}$, supportive of exposure to different environments during early life and segregation either side of a population boundary at the time of capture. This evidence of structuring discounted a single regional population; and equally, a single circumpolar population associated with the Current. Instead, consistent with predictions by Zhu et al. (2018), the results can be explained by a regional self-recruiting population associated with retention over the southern Kerguelen Plateau and fish from another population associated with eastward transport along the Current, in which $MgCa^{-1}$ was the single strongest marker separating the two groups.

$MgCa^{-1}$ additionally provided evidence of structuring at the otolith edge, in

chemistry laid down just before capture. As in the nucleus, fish from the AZ-SKP showed higher concentrations than those from the AZ-ACC/FTC. MgCa^{-1} previously distinguished between shelf environments characterized by different mixtures of Circumpolar Deep Water (Ashford et al. 2010), suggesting that versions of Circumpolar Deep Water around the Southern Ocean influence the rate of otolith deposition. However, Mg is conservative in seawater, and differences in salinity between water masses are small in the Antarctic. Instead, otolith MgCa^{-1} is considered to reflect fish activities that directly influence physiology (e.g., Martin and Thorrold 2005). Reproduction, feeding and movement are thought to contribute, modified by responses to spatially variable water properties between water masses (Ashford et al. 2005; Zhu et al. 2018; Caccavo et al. 2019). The moderated the Current signature over the southern Kerguelen Plateau (Bestley et al. 2018), quiescent water, slow anticyclonic drift (Supporting information Figure S1b) and moderate productivity (Supporting information Figure S1c) may influence activity and feeding behavior. The high concentrations at MIDOC Station 21 are consistent with this conclusion. For fish farther north on the southern Kerguelen Plateau (especially at MIDOC Station 23), Sea Surface Height streamlines and float trajectories indicated these were nearer the edge of the retention area, more likely to be influenced by water from oceanic areas in the Current further west (Supporting information Figure S1a). Further work is needed on a mechanistic explanation; nevertheless, the edge chemistry provides empirical evidence associating conditions over the southern Kerguelen Plateau with strong deposition of MgCa^{-1} .

Unusually for a fully marine species, the high levels of MgCa^{-1} in the nucleus chemistry of southern Kerguelen Plateau fish completely separated them from fish in the Current along the relationship with SrCa^{-1} . Criteria defining the separation showed zero error in the cross-validation, suggesting a population marker for the AZ-SKP fish relative to those in the Current. Several fish in the test data carried nucleus chemistry corresponding to the southern Kerguelen Plateau (Figure 8), consistent with connectivity eastward along the Current predicted by Zhu et al. (2018). The southern Kerguelen Plateau-allocated fish found in the Western Boundary Current suggested mixing from the retention area into the Current along the southeastern edge of the plateau; the two southern Kerguelen Plateau-allocated fish sampled from the Australia-Antarctic Gyre suggested entrainment southward after following the meanders east of the Western boundary Current.

Further questions arise when these results are compared with Zhu et al. (2018). Most fish they caught in the Current showed a similar relationship between MgCa^{-1} and SrCa^{-1} to AZ-ACC/FTC fish in our study (Figure 8). High MgCa^{-1} in two fish was originally attributed to sample variation, but their nucleus chemistry occupied multivariate space that in our study defines southern Kerguelen Plateau fish. By contrast, fish in the Antarctic Slope Current generally showed much lower concentrations of MgCa^{-1} (all < 125 ppm) that suggested a population distinct from both the southern Kerguelen Plateau and the Current. Moreover, three fish caught in

the Current showed nucleus chemistry indicative of Antarctic Slope Current origin.

Although intriguing, these comparisons warrant caution. Sample sizes were small and cross-study effects potentially introduced error and bias. Samples from the two studies were analyzed at two different times, in two different facilities, with different machine configurations and settings. Further investigation is necessary that accounts for the confounding variables by using a training set that incorporates all groups of interest in a single design. Strong between-area discrimination in each study suggests the potential for a comprehensive marker to identify fish from the Antarctic Slope Current as well as southern Kerguelen Plateau and the Current, but to define the groups accurately, the training set would depend on sampling at times or in areas characterized by no mixing and full separation of the populations of origin. Nevertheless, this study demonstrates the concept: a comprehensive training set with larger test samples could potentially allow estimation of the proportions mixing between populations along transport pathways. Separation into the component proportions facilitates multi-disciplinary testing including genetics. More generally, it helps determine the contributions different populations make to fish assemblages, and their association with features of interest in the large-scale circulation.

Population structuring along the Current

Important spatial asymmetries focus key physical processes in ‘hot spots’ where

the Current encounters topographic obstacles to its eastward flow (Rintoul 2018, their Figure 2). In the regime upstream, flow is largely zonal, fronts are distinct, and there is weak meridional eddy advection and weak cross-front exchange. On encountering the obstacle, vorticity constraints due to the shortening of the water column turn the jets equatorward and drive upwelling. Topographic steering causes jets to converge, steepening isopycnals, and the sloping bathymetry provides a stabilizing influence causing water to flow along the contours, helping to navigate meridionally around the obstacle. Downstream, as the Current crosses from shallow to deep, currents are turned poleward. The flow becomes destabilized, meandering is pronounced and there is rapid formation and growth of eddies. Strong poleward advection, stirring, and cross-front exchange result; fronts meander, split and merge, and the downstream regime is marked by vigorous upwelling along isopycnals steepened as a result of the convergence necessary to navigate the obstacle. The eddies reach a maximum downstream, before predominantly zonal flow is gradually reestablished.

The otolith chemistry helps place the population structuring and connectivity of *E. antarctica* into this system context. With oceanographic data from the Kerguelen Axis survey, it provides evidence to support a spatially stable, self-recruiting population occupying an area over the southern Kerguelen Plateau separated from the main Current flow steering around the topography. Particle tracking experiments (Mori et al. 2019) showed retention effects over the southern Kerguelen Plateau, and residence times ranging between 421 - 1075 days from Argo float trajectories

(Supporting information Figure S1c, Bestley et al. 2018) would allow eggs and larvae to remain over the period of development. This interpretation aligns with a recent proposal that pelagic squid species may use the southern Kerguelen Plateau as a spawning and nursery ground (Lin et al. 2019). As fish larvae mature, small adjustments in position during feeding would be expected to reinforce retention and survival over the plateau where productivity is relatively higher, and mitigate mortality and advective losses into less productive, fast-flowing areas of the Current, allowing a local spawning population to persist over the southern Kerguelen Plateau. The preponderance of males caught suggests further local structuring, possibly through behavior related to features in the mesoscale circulation intercepted by our sampling. However, loss of fish into the Current flows, potentially into the southern branch of Southern Antarctic Circumpolar Current Front via mesoscale eddy activity along the southern edge of the plateau (Bestley et al. 2018, their Supplementary material A2 video), may help explain the southern Kerguelen Plateau fish captured in the Western boundary Current and Australia-Antarctic Gyre. Simulations also indicate that a proportion of particles are transported eastward, especially from the eastern and southern flanks of the southern Kerguelen Plateau (Mori et al. 2019). By determining their meridional position downstream, the precise pathway off the plateau is likely to influence connectivity eastward along the Current, and southward towards the continental slope.

The nucleus chemistry indicated a separate origin for fish occupying the main

Current flows navigating around the southern Kerguelen Plateau. Fish associated with the northern branch of the Southern Antarctic Circumpolar Current Front, those exiting the Fawn Trough in the Fawn Trough Current, and four in the Western Boundary Current, exhibited similar chemistry. Meridional movement of Southern Antarctic Circumpolar Current Front branches around the southern Kerguelen Plateau leads to convergence with the southern Polar Front in the Fawn Trough, as well as the Southern Boundary in the Princess Elizabeth Trough, creating opportunities for fish to mix and move across fronts. In the downstream regime, enhanced eddy activity, meandering and vigorous upwelling lead to a dynamic, productive environment with enhanced opportunities for feeding (Schallenberg et al. 2018; Bestley et al. 2019), local retention, and meridional movement and mixing between fronts and potential transport pathways. Farther east where eddies dissipate, zonal transport suggests the potential for strong connectivity along fronts of the Current as envisaged by Zhu et al. (2018), until flows encounter further topographic obstacles (e.g. the Macquarie Ridge) where a similar general pattern of biophysical interactions can be expected to repeat. Indeed, transport from an area of high cross-frontal exchange farther west may help explain the similarity between fish captured in the AZ-ACC, the AZ-FTC (where the water properties indicated a Polar Front influence) and the Western Boundary Current. Topography farther west (e.g., the Southwest Indian Ridge, 20 ° E – 40 ° E) may enhance opportunities for cross-frontal exchange by steering flow, co-locating fronts and creating a region of high eddy activity (Sokolov and Rintoul 2009 a, b, their Figures 2, 7, 12). Many fish we sampled were 3 years or older (Table 2),

allowing sufficient time for transport from similar dynamic regions in the southern Atlantic Ocean and off the Antarctic Peninsula, where *E. antarctica* larvae occur in large numbers associated with versions of the Circumpolar Deep Water distinct from the southern Kerguelen Plateau.

No AZ-ACC fish were found with those over the southern Kerguelen Plateau, however. Connectivity along the Current did not appear to translate into immigration, despite a possible slow transport pathway along T9 (via the -1.05 m streamline, Figure 3a) onto the shallower parts of BANZARE Bank from oceanic areas farther west (Bestley et al. 2018). Larger sample sizes may yet reveal small numbers of immigrants into the southern Kerguelen Plateau population, but AZ-ACC fish may position themselves in the Current in a way that avoids areas of mixing, to remain in the northern branch of the Southern Antarctic Circumpolar Current Front. Alternatively, immigrants may simply be distributed patchily, associated with eroding the Current eddies over the southern Kerguelen Plateau in spatial concentrations that our biological sampling did not capture. Recently, a multidisciplinary approach used otolith chemistry and genetics to demonstrate structuring of Antarctic silverfish and strong gene flow along the Antarctic Slope Current (Caccavo et al. 2018, 2019). Strong differences between regional variations of the Circumpolar Deep Water around the Southern Ocean augur well for discriminating the origin of AZ-ACC fish, and genetics may help resolve how much immigration occurs over the southern Kerguelen Plateau. Measures of gonad maturity and fecundity would be valuable additions to a

multidisciplinary approach, as for silverfish (La Mesa et al. 2014). With larger sample sizes and a more comprehensive spatial design, the population marker carried in the nucleus chemistry can help to understand immigration, by estimating rates and their relationship to the circulation features used to enter the population. As Zhu et al. (2018) proposed, the large-scale circulation may shape population distributions of *E. antarctica* at circumpolar scales. Nevertheless, our results emphasize that biophysical mechanisms operating at the regional and meso-scales are likely to be fundamental in understanding the dynamics of self-recruiting populations structured by topographic barriers around the Southern Ocean.

References

- Ainley, D.G., W.R. Fraser, C.W. Sullivan, J.J. Torres, T.L. Hopkins, and W.O. Smith. 1986. Antarctic Mesopelagic Micronekton: Evidence from Seabirds that Pack Ice Affects Community Structure. *Science* **232**: 847-849. doi: 10.1126/science.232.4752.847
- Andriashev, A.P. 1965. A General Review of the Antarctic Fish Fauna. In: van Mieghem, J., P. van Oye (eds.) *Biogeography and Ecology in Antarctica*. Springer, Netherlands: 491-550. doi: 10.1007/978-94-015-7204-0_15
- Ashford, J.R., A.I. Arkhipkin, and C.M. Jones. 2006. Can the chemistry of otolith nuclei determine population structure of Patagonian toothfish *Dissostichus eleginoides*? *J. Fish. Biol.* **69**: 708-721. doi: 10.1111/j.1095-8649.2006.01144.x
- Ashford, J.R., A.I. Arkhipkin, and C.M. Jones. 2007. Otolith chemistry reflects frontal systems in the Antarctic Circumpolar Current. *Mar. Ecol. Prog. Ser.* **351**: 249-260. doi: 10.3354/meps07153
- Ashford, J.R., B.A. Fach, A.I. Arkhipkin, and C.M. Jones. 2012a. Testing early life connectivity supplying a marine fishery around the Falkland Islands. *Fish. Res.* **121**: 144-152. doi: 10.1016/j.fishres.2012.01.023
- Ashford, J.R., C. Jones, E. Hofmann, I. Everson, C. Moreno, G. Duhamel, and R. Williams. 2008. Otolith chemistry indicates population structuring by the Antarctic Circumpolar Current. *Can. J. Fish. Aquat. Sci.* **65**: 135-146. doi: 10.1139/F07-158
- Ashford, J.R., C.M. Jones, E.E. Hofmann, I. Everson, C. Moreno, G. Duhamel, and R.

- Williams. 2005. Can otolith elemental signatures record the capture site of Patagonian toothfish (*Dissostichus eleginoides*), a fully marine fish in the Southern Ocean? *Can. J. Fish. Aquat. Sci.* **62**: 2832-2840. doi: 10.1139/f05-191
- Ashford, J.R., M. Dinniman, C. Brooks, A.H. Andrews, E. Hofmann, G. Cailliet, C. Jones, and N. Ramanna. 2012b. Does large-scale ocean circulation structure life history connectivity in Antarctic toothfish (*Dissostichus mawsoni*)? *Can. J. Fish. Aquat. Sci.* **69**: 1903-1919. doi:10.1139/f2012-111
- Ashford, J.R., M. La Mesa, B. A. Fach, C. Jones, and I. Everson. 2010. Testing early life connectivity using otolith chemistry and particle-tracking simulations. *Can. J. Fish. Aquat. Sci.* **67**: 1303-1315. doi: 10.1139/F10-065
- Bestley, S., E. van Wijk, M. Rosenberg, R. Eriksen, S. Corney, K. Tattersall, and S. Rintoul. 2018. Ocean circulation and frontal structure near the southern Kerguelen Plateau: the physical context for the Kerguelen Axis ecosystem study. *Deep-Sea Res. PT. II* **174**: 104479. doi: 10.1016/j.dsr2.2018.07.013
- Bestley, S., V. Andrews-Goff, E. van Wijk, S.R. Rintoul, M.C. Double, and J. How. 2019. New insights into prime Southern Ocean forage grounds for thriving Western Australian humpback whales. *Sci. Rep.* **9**: 13988. doi: 10.1038/s41598-019-50497-2
- Bindoff, N.L., M.A. Rosenberg, and M.J. Warner. 2000. On the circulation and water masses over the Antarctic continental slope and rise between 80 and 150°E. *Deep-Sea Res. PT. II* **47**: 2299-2326. doi: 10.1016/S0967-0645(00)00038-2
- Caccavo, J.A., C. Papetti, M. Wetjen, R. Knust, J.R. Ashford, and L. Zane. 2018.

- Along-shelf connectivity and circumpolar gene flow in Antarctic silverfish (*Pleuragramma antarcticum*). *Sci. Rep.* **8**: 17856. doi: 10.1038/s41598-018-36030-x
- Caccavo, J.A., J.R. Ashford, S. Ryan, C. Papetti, M. Schroder, and L. Zane. 2019. Spatial structuring and life history connectivity of Antarctic silverfish along the southern continental shelf of the Weddell Sea. *Mar. Ecol. Prog. Ser.* **624**: 195-212. doi: 10.3354/meps13017
- Campana, S.E. 1999. Chemistry and composition of fish otoliths: pathways, mechanisms and applications. *Mar. Ecol. Prog. Ser.* **188**: 263-297. doi: 10.3354/meps188263
- Clarke, L., R. Trebilco, A. Walters, A.M. Polanowski, and B.E. Deagle. 2018. DNA-based diet analysis of mesopelagic fish from the southern Kerguelen Axis. *Deep-Sea Res. PT. II* **174**: 104404. doi: 10.1016/j.dsr2.2018.09.001
- Collins, M.A., G. Stowasser, S. Fielding, R. Shreeve, J.C. Xavier, H.J. Venables, P. Enderlein, Y. Cherel, and A.P. Van de Putte. 2012. Latitudinal and bathymetric patterns in the distribution and abundance of mesopelagic fish in the Scotia Sea. *Deep-Sea Res. PT. II* **59**: 189-198. doi:10.1016/j.dsr2.2011.07.003
- Dinniman M.S., and J.M. Klinck. 2004. A model study of circulation and cross shelf exchange on the west Antarctic Peninsula continental shelf. *Deep-Sea Res. PT. II* **51**: 2003-2022. doi: 10.1016/j.dsr2.2004.07.030
- Donnelly, J., and J.J. Torres. 2008. Pelagic fishes in the Marguerite Bay region of the west Antarctic Peninsula continental shelf. *Deep-Sea Res. PT. II* **55**: 523-539.

doi: 10.1016/j.dsr2.2007.11.015

Duhamel, G., P.A. Hulley, R. Causse, P. Koubbi, M. Vacchi, P. Pruvost, S. Vigetta, J.O. Irisson, S. Mormède, M. Belchier, A. Dettai, H. W. Detrich, J. Gutt, C. D. Jones, K.H. Kock, L.J. Lopez Abellan, and A.P. Van de Putte. 2014. Biogeographic patterns of fish. Science Committee of Antarctic Research, Cambridge: 327–362.

Efremenko, V.N. 1983. Atlas of fish larvae of the Southern Ocean. *Cybium* 7: 3-74.

Elsdon, T.S., B.K. Wells, S.E. Campana, B. M. Gillanders, C.M. Jones, K.E. Limburg, D.H. Secor, S.R. Thorrold, and B.D. Walther. 2008. Otolith chemistry to describe movements and life-history parameters of fishes. *Oceanogr. Mar. Biol.* 46: 297-330. doi: 10.1201/9781420065756.ch7

Flores, H., A.P. V. de Putte, V. Siegel, E.A. Pakhomov, J.A. Van Franeker, H.W.G. Meesters, and F.A.M. Volckaert. 2008. Distribution, abundance and ecological relevance of pelagic fishes in the Lazarev Sea, Southern Ocean. *Mar. Ecol. Prog. Ser.* 367: 271-282. doi: 10.3354/meps07530

Heywood, K.J., M.D. Sparrow, J. Brown, and R.R. Dickson. 1999. Frontal structure and Antarctic Bottom Water flow through the Princess Elizabeth Trough, Antarctica. *Deep-Sea Res. PT. I* 46: 1181-1200. doi: 10.1016/S0967-0637(98)00108-3

Hoddell, R.J., A.C. Crossley, R. Williams, and G. W. Hosie. 2000. The distribution of Antarctic pelagic fish and larvae (CCAMLR Division 58.4.1). *Deep-Sea Res. PT. II* 47: 2519-2541. doi: 10.1016/S0967-0645(00)00034-5

- Hu, Z.C., W. Zhang, Y.S. Liu, S. Gao, M. Li, K.Q. Zong, H.H. Chen, and S.H. Hu. 2015. "Wave" signal smoothing and mercury removing device for laser ablation quadrupole and multiple collector ICP-MS analysis: application to lead isotope analysis. *Analyt. Chem.* **87**: 1152-1157. doi: 10.1021/ac503749k
- Hulley, P.A., and G. Duhamel. 2011. Aspects of Lanternfish Distribution in the Kerguelen Plateau Region. In: Duhamel, G., Welsford, D. (eds.). *The Kerguelen Plateau: Mar. Ecosy. Fish. Société Française d'Ichtyologie*, Paris. 183-195. doi:10.13140/2.1.3870.1765
- Hulley, P.A., P. Camus, and G. Duhamel. 1989. Ichthyological results of cruise MD-42/SIBEX-II. Part 1. Fishes from RMT-8 stations, with additional records of lanternfishes (Myctophidae: Osteichthyes) from the Indian and Atlantic sectors of the Southern Ocean. *Cybiurn* **13**: 83-99.
- Hureau, J.C. 1994. The significance of fish in the marine Antarctic ecosystems. *Polar Biol.* **14**: 307-313. doi: 10.1007/BF00238445
- Izzo, C., P. Reis-Santos, and B.M. Gillanders. 2018. Otolith chemistry does not just reflect environmental conditions: A meta-analytic evaluation. *Fish Fish.* **19**: 441-454. doi: 10.1111/faf.12264
- Kellermann, A., and K.H. Kock. 1988. Patterns of spatial and temporal distribution and their variation in early life stages of Antarctic fish in the Antarctic Peninsula region. In: Sahrhage, D. (ed.), *Antarctic Ocean and Resources Variability*. Springer 147-159. doi: 10.1007/978-3-642-73724-4_12
- Kellermann, A., and S. Schadwinkel. 1991. Winter aspects of the ichthyoplankton

- community in Antarctic Peninsula waters. *Polar Biol.* **11**: 117-127. doi: 10.1007/BF00234274
- Khattree, R., and D.N. Naik. 1999. Applied multivariate statistics with SAS software. *Technometrics* **38**: 300. doi: 10.2307/1270637
- Khattree, R., and D.N. Naik. 2000. Multivariate data reduction and discrimination with SAS software. SAS Institute Inc., Cary, North Carolina, and John Wiley & Sons, New York.
- Kuehl, R.O. 1994. Statistical principles of research design and analysis. Duxbury Press, Belmont, California.
- Lea, M.A., P.D. Nichols, and G. Wilson. 2002. Fatty acid composition of lipid-rich myctophids and mackerel icefish (*Champsocephalus gunnari*) - southern ocean food-web implications. *Polar Biol.* **25**: 843-854. doi: 10.1007/s00300-002-0428-1
- Lin, D.M., A. Walters, S. Bestley, G.P. Zhu, X.J. Chen, and R. Trebilco. 2019. Distribution of larval and juvenile pelagic squids in the Kerguelen Axis region: Oceanographic influence on size structure and evidence of spawning locations. *Deep-Sea Res. PT. II* **174**: 104615. doi: 10.1016/j.dsr2.2020.104615
- Liu, Y.S., S. Gao, Z.C. Hu, C.G. Gao, K.Q. Zong, and D.B. Wang. 2010. Continental and oceanic crust recycling-induced melt-peridotite interactions in the Trans-North China Orogen: U-Pb dating, Hf isotopes and trace elements in zircons of mantle xenoliths. *J. Petrol.* **51**: 537-571. doi: 10.1093/petrology/egp082
- Liu, Y.S., Z.C. Hu, S. Gao, D. Günther, J. Xu, C.G. Gao, and H.H. Chen. 2008. In situ

- analysis of major and trace elements of anhydrous minerals by LA-ICP-MS without applying an internal standard. *Chem. Geol.* **257**: 34-43. doi: 10.1016/j.chemgeo.2008.08.004
- Loots, C., P. Koubbi, and G. Duhamel. 2007. Habitat modelling of *Electrona antarctica*, (Myctophidae, Pisces) in Kerguelen by generalized additive models and geographic information systems. *Polar Biol.* **30**: 951-959. doi: 10.1007/s00300-007-0253-7
- Martin G.B., and S.R. Thorrold. 2005. Temperature and salinity effects on magnesium, manganese and barium incorporation in otoliths of larval and early juvenile spot *Leiostomus xanthurus*. *Mar. Ecol. Prog. Ser.* **293**: 223-232. doi: 10.3354/meps293223
- McCartney, M.S., and K.A. Donohue. 2007. A deep cyclonic gyre in the Australian–Antarctic Basin. *Prog. Oceanogr.* **75**: 675-750. doi: 10.1016/j.pocean.2007.02.008
- Meijers, A.J.S., A. Klocker, N.L. Bindoff, G.D Williams, and S.J. Marsland. 2010. The circulation and water masses of the Antarctic shelf and continental slope between 30 and 80 °E. *Deep-Sea Res. PT. II* **57**: 723-737. doi: 10.1016/j.dsr2.2009.04.019
- Mori M., K. Mizobata, T. Okuda, and T. Ichii. 2019. Modelling egg and larval transport of Antarctic toothfish (*Dissostichus mawsoni*) in the East Antarctic region: preliminary result using satellite data. Selected Report of the Commission for the Conservation of Antarctic Marine Living Resources. Hobart,

- Australia. WG-FSA-2019/63.
- Moteki, M., K. Fujii, K. Amakasu, K. Shimada, A. Tanimura, and T. Odate. 2017. Distributions of larval and juvenile-adult stages of *Electrona antarctica*, off Wilkes Land in East Antarctic. *Polar Sci.* **12**: 99-108. doi: 10.1016/j.polar.2017.02.004
- Moteki, M., N. Horimoto, R. Nagaiwa, K. Amakasu, T. Ishimaru, and Y. Yamaguchi. 2009. Pelagic fish distribution and ontogenetic vertical migration in common mesopelagic species off Lützow-Holm Bay (Indian Ocean sector, Southern Ocean) during austral summer. *Polar Biol.* **32**: 1461-1472. doi: 10.1007/s00300-009-0643-0
- Nicol, S., T. Pauly, N.L. Bindoff, S. Wright, D. Thiele, G. W. Hosie, P.G. Strutton, and E. Woehler. 2000. Ocean circulation off East Antarctica affects ecosystem structure and sea-ice extent. *Nature* **406**: 504-507. doi: 10.1038/35020053
- North, A.W. 1987. Distribution of Fish Larvae at South Georgia Horizontal, Vertical, and Temporal Distribution and Early Life History Relevant to Monitoring Year-class Strength and Recruitment. Commission for the Conservation of Antarctic Marine Living Resources. Mimeograph. WG-FSA-87/16.pp. 19.
- Orsi, A.H., and C.L. Wiederwohl. 2009. A recount of Ross Sea waters. *Deep-Sea Res. II* **56**, 778-795. doi:10.1016/j.dsr2.2008.10.033
- Orsi, A.H., T. Whitworth, and W.D. Nowlin. 1995. On the meridional extent and fronts of the Antarctic Circumpolar Current. *Deep-Sea Res. PT. I* **42**: 641-673. doi: 10.1016/0967-0637(95)00021-W

- Pakhomov, E.A., R. Perissinotto, and C.D. McQuaid. 1996. Prey composition and daily rations of myctophid fishes in the Southern Ocean. *Mar. Ecol. Prog. Ser.* **134**: 1-14. doi: 10.3354/meps134001
- Park, Y.-H., Vivier, F., Roquet, F., Kestenare, E., 2009. Direct observations of the ACC transport across the Kerguelen Plateau. *Geophys. Res. Lett.* **36**: L18603.
- Parker, M.L., W.R. Fraser, J. Ashford, T. Patarnello, L. Zane, and J.J. Torres. 2015. Assemblages of micronektonic fishes and invertebrates in a gradient of regional warming along the Western Antarctic Peninsula. *J. Marine. Syst.* **152**: 18-41. doi: 10.1016/j.jmarsys.2015.07.005
- Patterson, H.M., M.J. Kingsford, and M.T. Mcculloch. 2005. Resolution of the early life history of a reef fish using otolith chemistry. *Coral Reefs* **24**: 222-229. doi: 10.1007/s00338-004-0469-8
- Riaz, J., A. Walters, R. Trebilco, S. Bestley, and M.A. Lea. 2019. Stomach content analysis of mesopelagic fish from the southern Kerguelen Axis. *Deep-Sea Res. PT. II* **174**: 104659. doi: 10.1016/j.dsr2.2019.104659
- Rintoul, S.R. 2018. The global influence of localized dynamics in the Southern Ocean. *Nature* **558**: 209-218. doi: 10.1038/s41586-018-0182-3
- Rintoul, S.R., C. Hughes, and D. Olbers. 2001. The Antarctic circumpolar system. In: Siedler, G., J. Church, and J. Gould (eds.). *Ocean Circulation and Climate – Observing and Modelling the Global Ocean*. Academic Press, Amsterdam: 271-302. doi: 10.1016/S0074-6142(01)80124-8
- Schallenberg, C., S. Bestley, A. Klocker, T.W. Trull, D.M. Davies, M. Gault-Ringold,

- R. Eriksen, N.P. Roden, S. Sander, M. Sumner, A.T. Townsend, P. van der Merwe, K. Westwood, K. Wuttig, and A. Bowie. 2018. Sustained upwelling of subsurface iron supplies seasonally persistent phytoplankton blooms around the southern Kerguelen plateau, Southern Ocean. *J. Geophys. Res. - Oceans.* **123**: 5986-6003. doi: 10.1029/2018JC013932
- Smith, D.A., Hofmann, E.E., Klinck, J.M., Lascara, C.M. 1999. Hydrography and circulation of the west Antarctic Peninsula continental shelf. *Deep-Sea Res. Part A Oceanogr. Res. Pap.*, 46, 925-949. 10.1016/S0967-0637(98)00103-4
- Sokolov, S., and S.R. Rintoul. 2009a. Circumpolar structure and distribution of the Antarctic Circumpolar Current fronts: 1. Mean circumpolar paths. *J. Geophys. Res. - Oceans.* **114**: C005108. doi: 10.1029/2008JC005108
- Sokolov, S., and S.R. Rintoul. 2009b. Circumpolar structure and distribution of the Antarctic Circumpolar Current fronts: 2. Variability and relationship to sea surface height. *J. Geophys. Res. - Oceans.* **114**: C005248. doi: 10.1029/2008JC005248
- Van de Putte, A.P., G.D. Jackson, E. Pakhomov, H. Flores, and F.A.M. Volckaert. 2010. Distribution of squid and fish in the pelagic zone of the Cosmonaut Sea and Prydz Bay region during the BROKE-West campaign. *Deep-Sea Res. PT. II* **57**: 956-967. doi: 10.1016/j.dsr2.2008.02.015
- Van Wijk, E.M., S.R. Rintoul, B.M. Ronai, and G.D. Williams. 2010. Regional circulation around Heard and McDonald Islands and through the Fawn Trough, central Kerguelen Plateau. *Deep-Sea Res. PT. I* **57**: 653-669. doi:

10.1016/j.dsr.2010.03.001

Weatherall, P., K.M. Marks, M. Jakobsson, T. Schmitt, S. Tani, J.E. Arndt, M.

Rovere, D. Chayes, V. Ferrini, and R. Wigley. 2015. A new digital bathymetric model of the world's oceans. *Earth Space Sci.* **2**: 331-345. doi: 10.1002/2015EA000107

Williams, G.D., S. Nicol, S. Aoki, A.J.S. Meijers, N.L. Bindoff, Y. Iijima, S.J.

Marsland, and A. Klocker. 2010. Surface oceanography of BROKE-WEST, along the Antarctic margin of the south-west Indian Ocean (30-80 ° E). *Deep-Sea Res. PT. II* **57**: 738-757. doi: 10.1016/j.dsr2.2009.04.020

Zhu, G.P., M. Duan, J.R. Ashford, L. Wei, M.X. Zhou, and S. Bestley. 2018. Otolith

nucleus chemistry distinguishes *Electrona antarctica* in the westward-flowing Antarctic Slope Front Current and eastward-flowing Antarctic Circumpolar Current off East Antarctica. *Mar. Environ. Res.* **142**: 7-20. doi: 10.1016/j.marenvres.2018.09.010

Zhu, G.P., M. Duan, L. Wei, R. Trebilco, S. Bestley, and A. Walters. 2020.

Determination and precision of otolith growth zone estimates of *Electrona antarctica* in the Southern Kerguelen Plateau region in the Indian sector of the Southern Ocean. *Deep-Sea Res. PT. II* **174**: 104778. doi: 10.1016/j.dsr2.2020.104778

Zong, K.Q., Y.S. Liu, C.G. Gao, Z.H. Hu, S. Gao, and H.J. Gong. 2010. In situ U-Pb

dating and trace element analysis of zircons in thin sections of eclogite: refining constraints on the UHP metamorphism of the Sulu Terrane. *China Chem. Geol.*

269: 237–251. doi: 10.1016/j.chemgeo.2009.09.02

Acknowledgements

We thank the Science Technical Support Team of the Australian Antarctic Division and the master and crew of the *Aurora Australis* for their considerable efforts to make this work happen. We are especially thankful for the assistance from grateful to Dr Rowan Trebilco from CSIRO Oceans and Atmosphere, Australia and Mr Dale Maschette on the K-AXIS fish sampling team from Australian Antarctic Division to collect the fish samples, as well as Brad Collins, Mick Stapleton and Danny Phillips for their tremendous efforts assisting with the onboard sampling. Dr. Trebilco also provided helpful comments to improve an earlier version of the paper. Our thanks also go to the chief scientist of this cruise, Dr Andrew Constable, for his invitation to participate. We thank Ms Hui Liu to for help producing Figure 1. This project was supported by the National Science Foundation of China (grant number 41776185 to GPZ), China's National Key Research and Development Project (grant number 2018YFC1406801 to GPZ), Chinese-Australian Young Scientist Exchange Program of China Association for Science and Technology (Cooperative Research in Antarctic Ecosystem, grant number 2020ZZGJB060926) and the Australian Government under the Australian Antarctic Science program (AAS Grant 4344). SB and AW were supported under the Australia Research Council's Special Research Initiative for Antarctic Gateway Partnership (Project ID SR140300001). SB also received support under DECRA award DE180100828. The authors declare that they have no conflict of interest.

Table 1. Information on sampling stations 34, 35, and 36, where midwater opening/closing (MIDOC) multiple cod-end device net was deployed, relating to depth, water mass properties and oceanic zone. The oceanic zone and water mass characterization follow Bestley et al. (2018). Abbreviations are MCDW: Modified Circumpolar Deep Water; LCDW: Lower Circumpolar Deep Water; UCDW: Upper Circumpolar Deep Water. CTD (conductivity-temperature-depth profiler) station numbers are given for cross-referencing to the oceanographic sampling reported in Bestley et al. (2018). Numbers give the observed ranges of water properties over each 200 m sampled layer, where Θ indicates potential temperature, S indicates salinity (on the practical salinity scale, PSS) and O₂ indicates dissolved oxygen (not available for depths > 400 m on transect 9).

MIDOC Station	Date	CTD Station	lat	lon	Depth (m)	Θ (°C)	S (PSS)	O ₂ (μ mol l ⁻¹)	Oceanic zone	Water mass
MIDOC 16	2016/2/4	23	-64.43	90.04	600-800	0.97- 1.13	34.717-34.721	206-208	Subpolar	LCDW
MIDOC 21	2016/2/6	29	-60.47	82.72	800-1000	1.26-	34.736-34.742	205-207	Antarctic	– LCDW

							1.45			SKP	
MIDOC 22	2016/2/7	30	-59.49	81.39	800-1000	1.25-	34.735-34.743	203-206	Antarctic	-	LCDW
							1.47			SKP	
MIDOC 23	2016/2/7	31	-58.78	80.32	800-1000	1.37-	34.740-34.746	203-206	Antarctic	-	LCDW
							1.57			SKP	
MIDOC 30	2016/2/11	38	-59.85	86.51	800-1000	1.56-	34.732-34.741	NA	Antarctic	-	LCDW
							1.75			FTC	
MIDOC 31	2016/2/11	39	-60.06	86.04	400-600	1.33-	34.689-	NA	Subpolar eddy		LCDW
							1.48	34.715*			
MIDOC 34	2016/2/13	42	-60.85	80.16	800-1000	1.58-	34.743-34.747	NA	Antarctic	-	LCDW
							1.75			ACC	
MIDOC 35	2016/2/14	43	-61.27	77.85	600-800	1.78-	34.718-34.739	NA	Antarctic	-	LCDW
							1.91			ACC	

MIDOC 36	2016/2/14	44	-61.79	74.43	200-400	1.92-	34.614-34.695	173-183	Antarctic	- UCDW
						1.95			ACC	

* Salinities >34.7 over more than 80% of the 200 m trawl layer.

Table 2. Summary information on *E. antarctica* (n=36) sampled for otoliths in this study.

Otolith code	Date	Statio n	Standard length(mm)	Age (year)	Sex
MIDOC16_3_07	2016/2/4	16	88.59	6	/
MIDOC16_3_08	2016/2/4	16	76.03	4	/
MIDOC16_3_09	2016/2/4	16	67.41	3	/
MIDOC16_3_11	2016/2/4	16	47.99	2	/
MIDOC21_2_16	2016/2/6	21	71.00	4	Male
MIDOC21_2_17	2016/2/6	21	56.00	3	Male
MIDOC21_2_29	2016/2/6	21	56.00	3	Male
MIDOC21_2_20	2016/2/6	21	61.00	3	Male
MIDOC21_2_21	2016/2/6	21	61.00	3	Female
MIDOC22_2_07	2016/2/7	22	92.46	6	Female
MIDOC22_2_08	2016/2/7	22	81.51	5	Male
MIDOC22_2_09	2016/2/7	22	43.64	2	/
MIDOC22_2_10	2016/2/7	22	59.50	3	Male
MIDOC22_2_11	2016/2/7	22	79.75	4	Male
MIDOC23_2_30	2016/2/7	23	74.94	4	Male
MIDOC23_2_31	2016/2/7	23	70.64	3	Male
MIDOC23_2_35	2016/2/7	23	74.80	4	Male
MIDOC23_2_36	2016/2/7	23	76.31	4	Male
MIDOC30_2_27	2016/2/11	30	103.49	7	Female

MIDOC30_2_28	2016/2/11	30	68.70	3	Female
MIDOC30_2_29	2016/2/11	30	58.41	2	Male
MIDOC30_2_31	2016/2/11	30	55.78	2	Female
MIDOC31_4_19	2016/2/11	31	80.88	4	Female
MIDOC31_4_20	2016/2/11	31	55.28	2	Male
MIDOC31_4_21	2016/2/11	31	35.09	1	Immature
MIDOC31_4_22	2016/2/11	31	60.86	4	Male
MIDOC31_4_23	2016/2/11	31	43.87	1	Immature
MIDOC34_2_23	2016/2/13	34	102.18	7	/
MIDOC34_2_24	2016/2/13	34	100.26	6	Female
MIDOC35_3_38	2016/2/14	35	102.92	7	Female
MIDOC35_3_40	2016/2/14	35	78.59	4	Male
MIDOC35_3_42	2016/2/14	35	60.60	3	Female
MIDOC36_5_32	2016/2/14	36	45.71	2	Immature
MIDOC36_5_19	2016/2/14	36	73	4	Female
MIDOC36_5_30	2016/2/14	36	42.61	2	Male
MIDOC36_5_31	2016/2/14	36	44.94	2	Male

Table 3. Average precision, detection limits and minimum observed concentrations in analysis of *E. antarctica* otoliths.

	⁷ Li	²⁴ Mg	⁴² Ca	⁵⁵ Mn	⁸⁸ Sr	¹³⁷ Ba
Detection limit (ppm)	0.661	0.413	265.453	0.779	0.273	0.009
Precision (%; 1 standard error)	0.180	0.085	50.784	0.139	0.820	0.033
Minimum concentration in nucleus (ppm)	<0.661	7.499	387689.2	<0.779	1741.339	0.920
Minimum concentration in edge (ppm)	<0.661	4.446	392661	<0.779	1712.384	0.780

Table 4. Concentrations of MgCa^{-1} ($\times 10^6$), SrCa^{-1} ($\times 10^3$), BaCa^{-1} ($\times 10^6$) in the nucleus and at the edge of otoliths from *E. antarctica*.

Otolith code	Otolith nucleus			Otolith edge		
	MgCa^{-1}	SrCa^{-1}	BaCa^{-1}	MgCa^{-1}	SrCa^{-1}	BaCa^{-1}
MIDOC16_3_07	110.209	5.745	3.463	18.424	4.777	3.942
MIDOC16_3_08	155.381	9.580	4.532	22.805	5.025	1.980
MIDOC16_3_09	107.459	4.432	3.541	24.523	6.236	2.575
MIDOC16_3_11	115.597	14.651	8.964	27.403	5.860	3.774
MIDOC21_2_16	493.333	8.096	9.246	58.066	5.087	2.603
MIDOC21_2_17	338.492	8.648	10.931	49.173	5.030	5.305
MIDOC21_2_29	587.422	7.734	4.785	89.667	5.797	3.753
MIDOC21_2_20	200.263	4.490	3.660	78.802	4.560	4.458
MIDOC21_2_21	665.105	12.483	4.329	64.597	4.441	2.970
MIDOC22_2_07	191.284	10.485	3.461	26.871	4.871	2.054
MIDOC22_2_08	161.729	5.898	3.933	19.358	7.152	2.055
MIDOC22_2_09	226.105	9.945	6.572	48.141	5.025	4.081
MIDOC22_2_10	361.115	9.168	6.841	23.577	6.356	4.995
MIDOC22_2_11	248.038	8.768	4.016	40.692	4.572	6.477
MIDOC23_2_30	134.719	6.871	3.865	28.932	7.085	5.389
MIDOC23_2_31	306.998	8.777	2.701	22.983	5.348	11.065
MIDOC23_2_35	122.669	5.087	3.463	24.756	5.385	2.734
MIDOC23_2_36	109.105	4.789	4.437	26.050	6.586	3.502

MIDOC30_2_27	48.158	4.870	4.270	16.664	5.345	6.115
MIDOC30_2_28	196.294	12.907	7.308	28.616	5.602	6.749
MIDOC30_2_29	95.266	7.617	3.925	30.205	4.731	4.962
MIDOC30_2_31	181.964	13.823	4.328	29.490	4.356	2.388
MIDOC31_4_19	121.779	11.073	11.665	22.161	5.005	5.937
MIDOC31_4_20	219.431	12.838	4.846	18.493	5.662	3.557
MIDOC31_4_21	336.035	7.875	4.208	20.662	5.211	3.307
MIDOC31_4_22	129.429	12.279	6.354	16.880	7.032	3.456
MIDOC31_4_23	146.046	9.551	3.043	31.078	4.523	3.253
MIDOC34_2_23	123.091	11.011	10.368	12.553	5.795	2.228
MIDOC34_2_24	32.964	5.675	4.074	22.539	4.348	2.880
MIDOC35_3_38	39.244	5.917	4.082	14.873	6.960	4.455
MIDOC35_3_40	37.886	4.468	2.331	11.308	7.739	3.584
MIDOC35_3_42	19.042	4.937	2.809	35.959	5.158	5.355
MIDOC36_5_32	73.597	7.022	3.675	24.603	4.988	2.598
MIDOC36_5_19	70.655	7.585	6.632	17.158	5.783	2.474
MIDOC36_5_30	74.989	7.914	3.110	14.414	5.229	2.524
MIDOC36_5_31	134.994	14.394	8.335	21.819	5.019	3.480

Table 5. Classification results from Multivariate Discriminant Analysis for test data from the Australian Antarctic Gyre (AAG, n=4) and Western Boundary Current (WBC, n=5) east of the southern Kerguelen plateau (SKP). Abbreviations are ACC: Antarctic Circumpolar Current; PR: Probability.

Otolith Code	Area of capture	of PR_SKP (%)	PR_ACC (%)	Classified to area
MIDOC16_3_07	AAG	88.034	11.966	SKP
MIDOC16_3_08	AAG	22.662	77.338	ACC
MIDOC16_3_09	AAG	97.942	2.058	SKP
MIDOC16_3_11	AAG	0.001	99.999	ACC
MIDOC31_4_19	WBC	0.073	99.927	ACC
MIDOC31_4_20	WBC	6.839	93.161	ACC
MIDOC31_4_21	WBC	99.988	0.012	SKP
MIDOC31_4_22	WBC	0.062	99.938	ACC
MIDOC31_4_23	WBC	30.253	69.747	ACC

Figure captions

Figure 1. Map of the Southern Ocean, showing the climatological position of the major Antarctic Circumpolar Current (ACC) fronts (following Orsi et al. 1995), the occurrence position (left panel) and occurrence probability (right panel) of *Electrona antarctica*. The data of occurrence probability and occurrence position for *E. antarctica* is derived from Fishbase (www.fishbase.org). Abbreviations are SACCF: Southern Antarctic Circumpolar Current Front, SAF: Sub-Antarctic Front, SB: Southern Boundary of the ACC, STF: Sub-Tropical Front, PF: Polar Front. The letters in left panel show place names referred to in the text, A: Lazarev Sea; B: Lützw-Holm Bay; C: SW Indian Ridge; D: Kerguelen Plateau; E: Prydz Bay; F: Wilkes Land; G: George V Shelf; H: Macquarie Ridge; I: Antarctic Peninsula; K: Scotia Sea; J: South Georgia.

Figure 2. Circulation schematic around the southern Kerguelen plateau (SKP) adapted from Bestley et al. (2018), showing the positions of stations where midwater opening/closing (MIDOC) multiple cod-end device net was deployed (numbered circles) sampled along transects T6 (north-south) and T9 (east-west). Major oceanographic features: Southern Antarctic Circumpolar Current Front (SACCF); Fawn Trough Current (FTC); Southern Boundary of the Antarctic Circumpolar Current (SB); and Antarctic Slope Front (ASF). Dashed lines indicate features inferred but not directly sampled by the hydrographic survey. Colour of MIDOC stations indicates oceanic zone following Bestley et al. (2018): Antarctic Zone corresponding to the Antarctic Circumpolar Current (red), Antarctic Zone over the SKP (orange) and Subpolar (blue). Note that Antarctic Zone corresponding to the FTC (black, station 30) is included as Antarctic Zone corresponding to the Antarctic Circumpolar Current

(red outline) for all analyses. Background displays bathymetry (Weatherall et al., 2015) at 500 m intervals, with 2000 m and 3000 m isobaths highlighted (white contours). Major geographical features are named, with the Antarctic continent and major ice features shown in grey and white, respectively.

Figure 3. Water properties from oceanographic sampling along zonal transect T9 (CTD Stations 38 - 44) and meridional transect T6 (CTD Stations 23, 29 - 31; see Table 1). Main panel a) shows potential temperature (Θ) – salinity, adapted from Fig. 5c-e in Bestley et al. (2018). Data in panels b-d) focus on the subsurface below 100 m and show b) dissolved oxygen – salinity curves, as well as c) dissolved oxygen, and d) potential temperature each in relation to neutral density (γ). Abbreviations are CTD: conductivity-temperature–depth profiler; AZ-ACC, Antarctic Zone corresponding to the Antarctic Circumpolar Current; AZ-SKP, Antarctic Zone over the south Kerguelen Plateau; AZ-FTC, Antarctic Zone corresponding to the Fawn Trough Current. Colour follows Figure 2.

Figure 4. Vertical oceanographic section along zonal transect T9 showing a) potential temperature ($0\text{ }^{\circ}\text{C}$), b) salinity (practical salinity scale, PSS), c) dissolved oxygen ($\mu\text{mol l}^{-1}$), d) neutral density (kg m^{-3}). Zonal transect runs approximately east-west across the southern Kerguelen Plateau. CTD (conductivity-temperature-depth profiler) stations 38-44 are numbered above each panel with dotted lines showing the depth limit of each cast. Note CTD station 41 sampled along T9 is a crossover pair with CTD station 29 (MIDOC 21, Table 1) sampled along T6. CTD station 40 was not sampled by fish trawl but is shown for completeness of survey transect. Vertical scale changes are indicated by the breaks in the y-axis. Labelled water masses: Lower Circumpolar Deep Water (LCDW), Upper Circumpolar Deep Water (UCDW), Antarctic Bottom Water (AABW). Location of western boundary current (WBC) along the eastern flank

near 85°E is also indicated. Bathymetry is derived from the ship's 12 kHz echosounder.

Figure 5. Otoliths of *E. antarctica* viewed under reflected light. Panels show the morphology of the a) sagittal otolith (whole otolith before sectioning), and b) transverse section of same otolith, showing translucent nucleus and spot rasters for laser ablation (red); 1: nucleus, 2: first translucent zone (age 0+), 3 – 4: translucent zones from age 1+ to age 2+, 5: edge of otolith transverse section (age 3+). Abbreviation is SL: standard length.

Figure 6. Concentrations of MgCa^{-1} ($\times 10^6$), SrCa^{-1} ($\times 10^3$), BaCa^{-1} ($\times 10^6$) from *E. antarctica* sampled from the southern Kerguelen Plateau (SKP) and Antarctic Circumpolar Current (ACC) a) in the nucleus and b) at the edge of otolith. Upper panel shows MgCa^{-1} against SrCa^{-1} ; lower panel shows MgCa^{-1} against BaCa^{-1} . Abbreviations are AZ-ACC: Antarctic Zone corresponding to the ACC; AZ-FTC: Antarctic Zone corresponding to the Fawn Trough Current.

Figure 7. Concentrations of MgCa^{-1} ($\times 10^6$), SrCa^{-1} ($\times 10^3$), BaCa^{-1} ($\times 10^6$) in the otolith nucleus of *E. antarctica* sampled from the Western Boundary Current (WBC) and Australia-Antarctic Gyre (AAG); compared to those from southern Kerguelen Plateau (SKP) and Antarctic Circumpolar Current (ACC) used in a training set for Discriminant Analysis. Upper panel shows MgCa^{-1} against SrCa^{-1} ; lower panel shows MgCa^{-1} against BaCa^{-1} . Border color for WBC and AAG indicates classification to SKP or ACC.

Figure 8. Otolith nucleus concentrations of MgCa^{-1} ($\times 10^6$), SrCa^{-1} ($\times 10^3$), BaCa^{-1} ($\times 10^6$) from *E. antarctica* sampled from the AZ-SKP and AZ-ACC/FTC in this study (circles), compared to samples from Zhu et al. (2018) in the ACC and ASC (crosses). Upper panel shows MgCa^{-1} against SrCa^{-1} ; lower panel shows MgCa^{-1} against BaCa^{-1} . Abbreviations are AZ-SKP: Antarctic Zone over the southern Kerguelen Plateau; AZ-ACC/FTC: Antarctic Zone

corresponding to the Antarctic Circumpolar Current and the Fawn Trough Current; ASC:

Antarctic Slope Current.

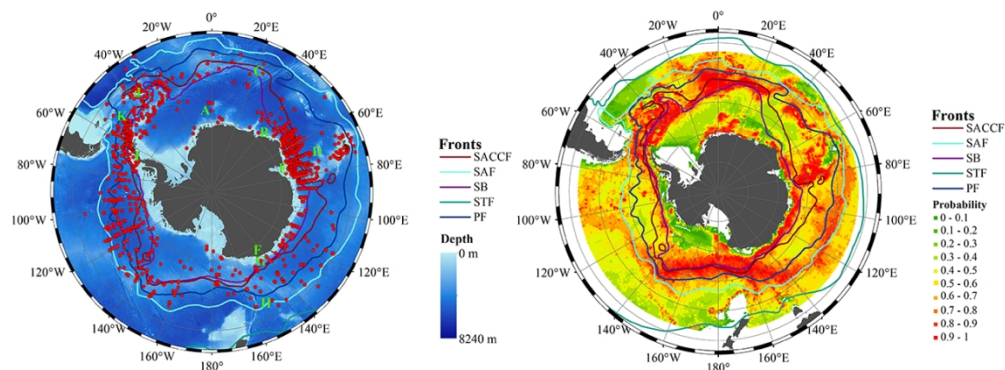
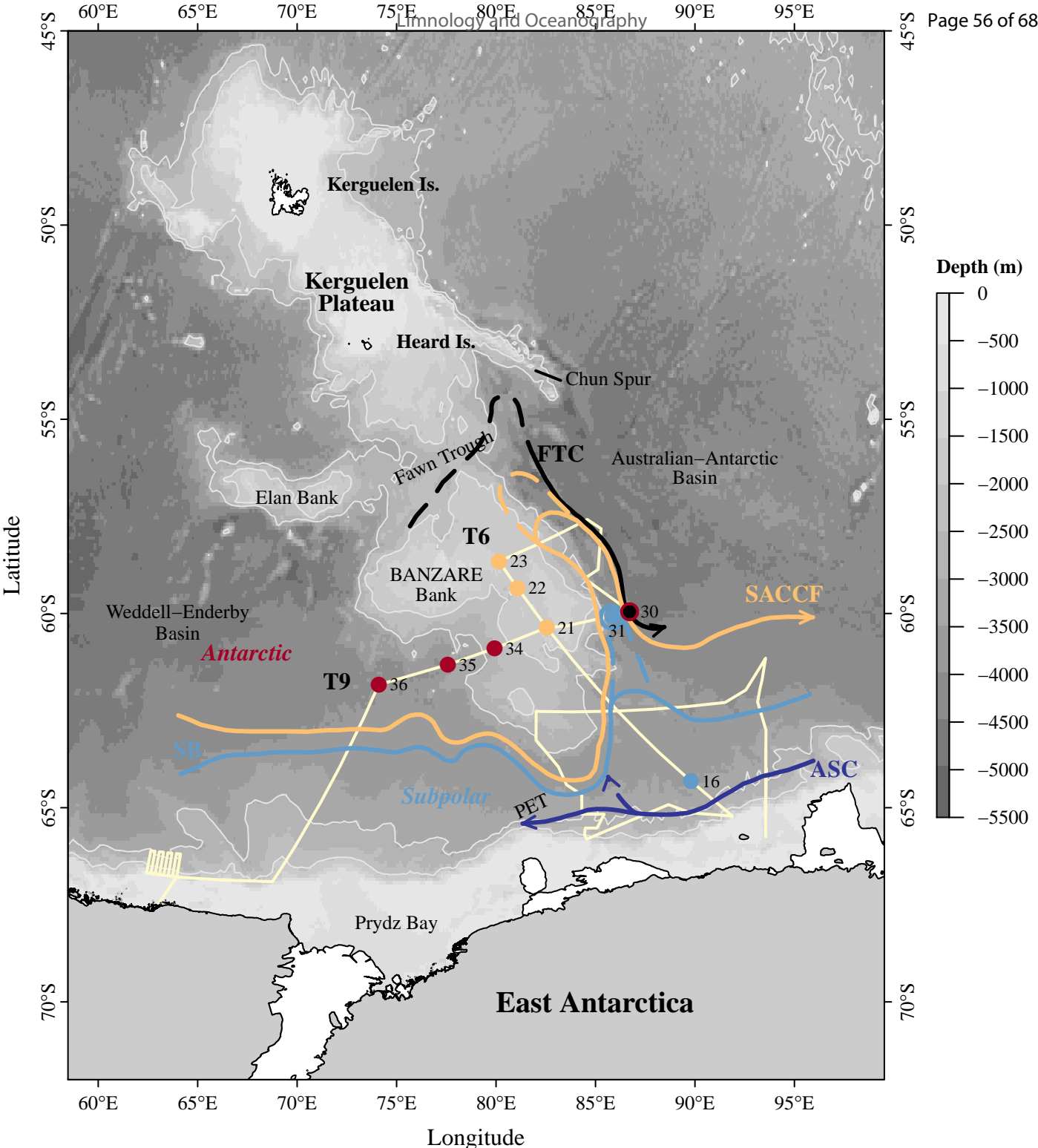


Figure 1. Map of the Southern Ocean, showing the climatological position of the major Antarctic Circumpolar Current (ACC) fronts (following Orsi et al. 1995), the occurrence position (left panel) and occurrence probability (right panel) of *Electrona antarctica*. The data of occurrence probability and occurrence position for *E. antarctica* is derived from Fishbase (www.fishbase.org). Abbreviations are SACCF: Southern Antarctic Circumpolar Current Front, SAF: Sub-Antarctic Front, SB: Southern Boundary of the ACC, STF: Sub-Tropical Front, PF: Polar Front. The letters in left panel show place names referred to in the text, A: Lazarev Sea; B: Lützow-Holm Bay; C: SW Indian Ridge; D: Kerguelen Plateau; E: Prydz Bay; F: Wilkes Land; G: George V Shelf; H: Macquarie Ridge; I: Antarctic Peninsula; K: Scotia Sea; J: South Georgia.

110x43mm (300 x 300 DPI)



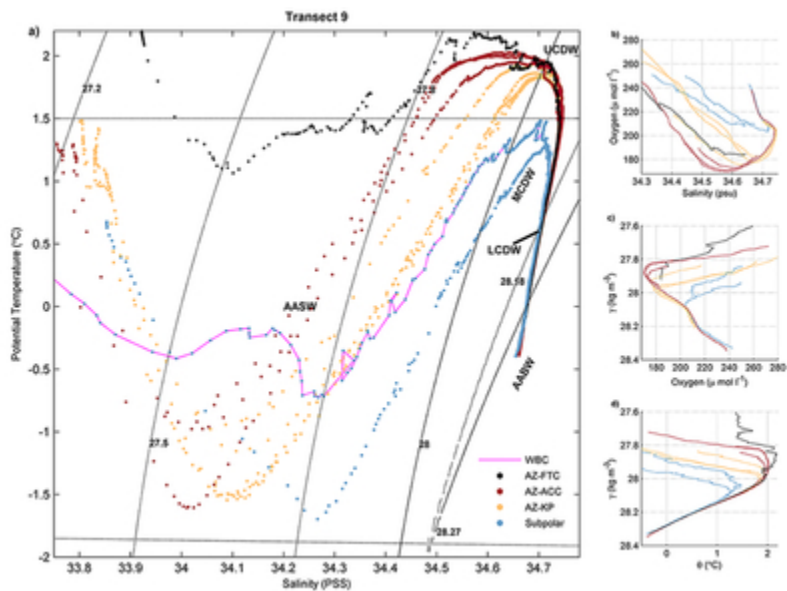


Figure 3. Water properties from oceanographic sampling along zonal transect T9 (CTD Stations 38 - 44) and meridional transect T6 (CTD Stations 23, 29 - 31; see Table 1). Main panel a) shows potential temperature (□) – salinity, adapted from Fig. 5c-e in Bestley et al. (2018). Data in panels b-d) focus on the subsurface below 100 m and show b) dissolved oxygen – salinity curves, as well as c) dissolved oxygen, and d) potential temperature each in relation to neutral density (γ). Abbreviations are CTD: conductivity-temperature–depth profiler; AZ-ACC, Antarctic Zone corresponding to the Antarctic Circumpolar Current; AZ-SKP, Antarctic Zone over the south Kerguelen Plateau; AZ-FTC, Antarctic Zone corresponding to the Fawn Trough Current. Colour follows Figure 2.

33x25mm (300 x 300 DPI)

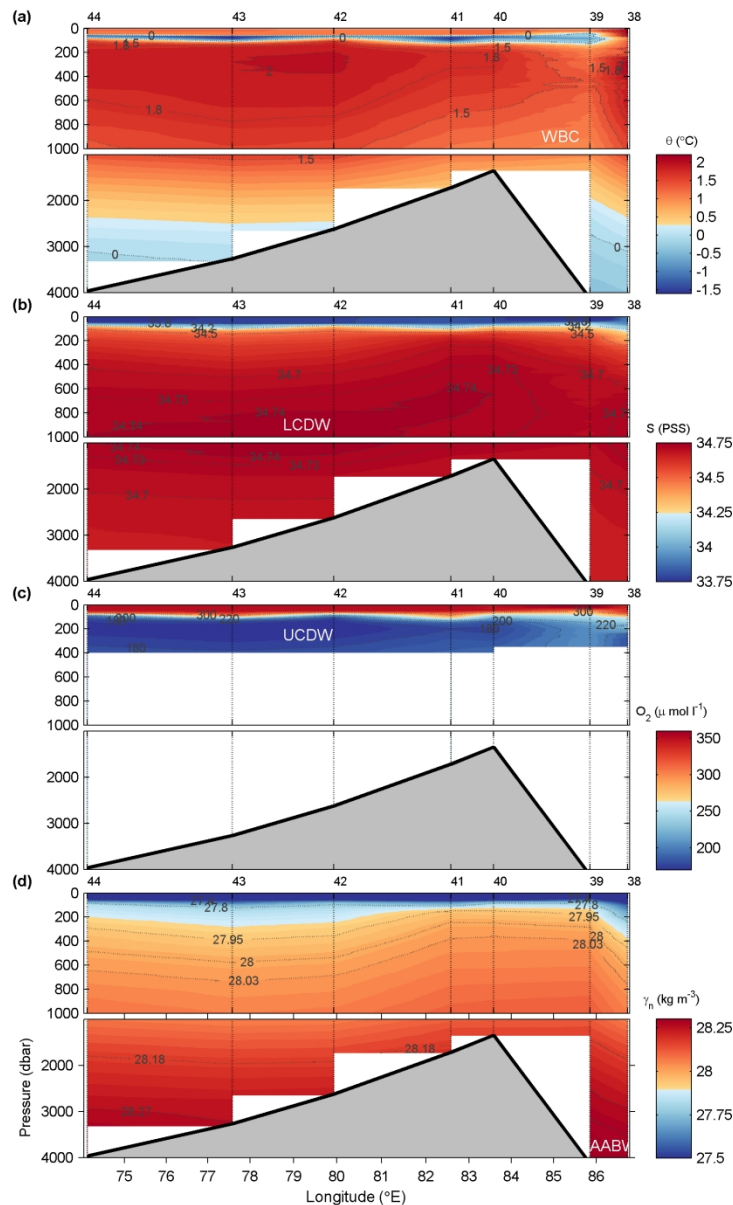


Figure 4. Vertical oceanographic section along zonal transect T9 showing a) potential temperature ($^{\circ}\text{C}$), b) salinity (practical salinity scale, PSS), c) dissolved oxygen ($\mu\text{mol l}^{-1}$), d) neutral density (kg m^{-3}). Zonal transect runs approximately east-west across the southern Kerguelen Plateau. CTD (conductivity-temperature-depth profiler) stations 38-44 are numbered above each panel with dotted lines showing the depth limit of each cast. Note CTD station 41 sampled along T9 is a crossover pair with CTD station 29 (MIDOC 21, Table 1) sampled along T6. CTD station 40 was not sampled by fish trawl but is shown for completeness of survey transect. Vertical scale changes are indicated by the breaks in the y-axis. Labelled water masses: Lower Circumpolar Deep Water (LCDW), Upper Circumpolar Deep Water (UCDW), Antarctic Bottom Water (AABW). Location of western boundary current (WBC) along the eastern flank near 85°E is also indicated. Bathymetry is derived from the ship's 12 kHz echosounder.

150x240mm (300 x 300 DPI)

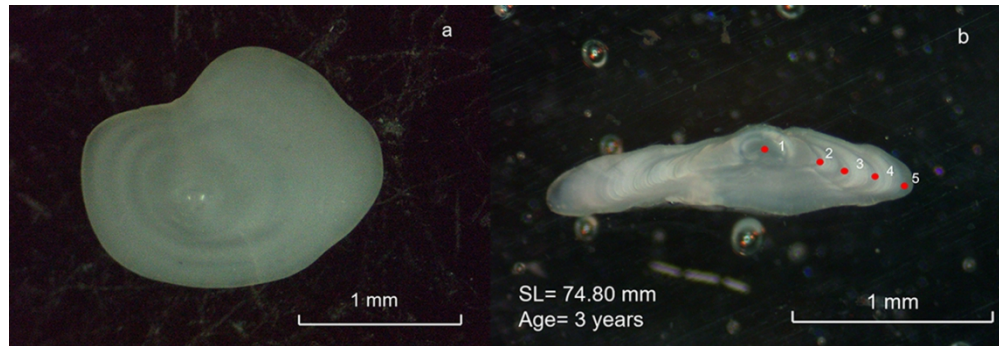
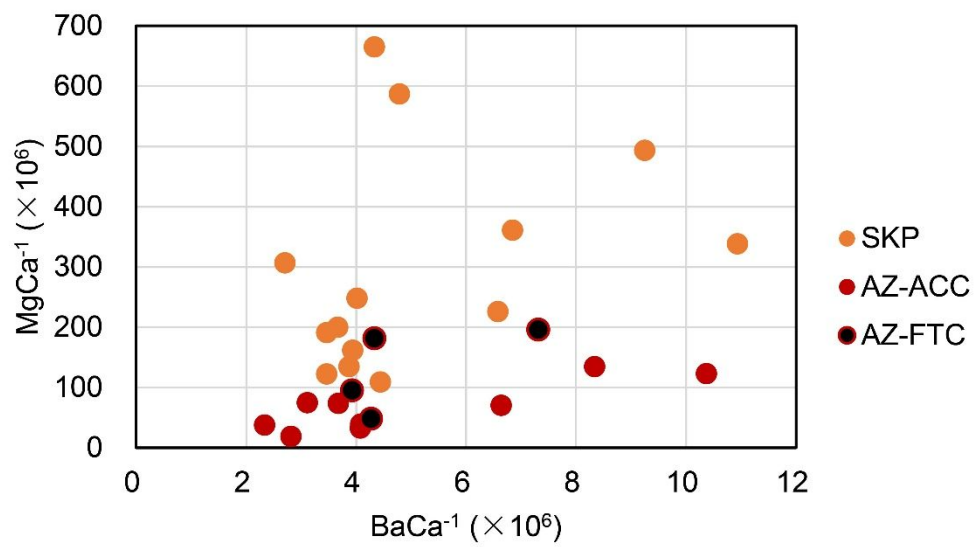
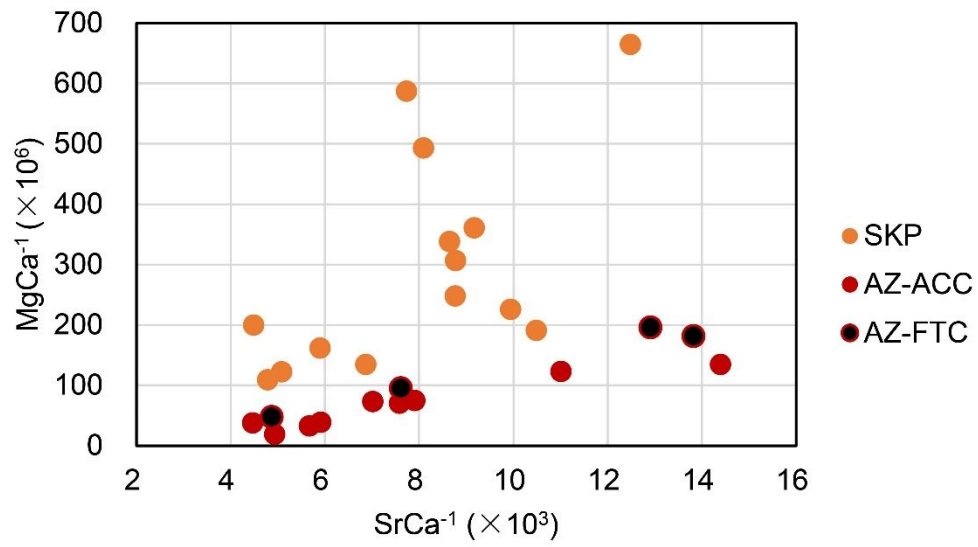


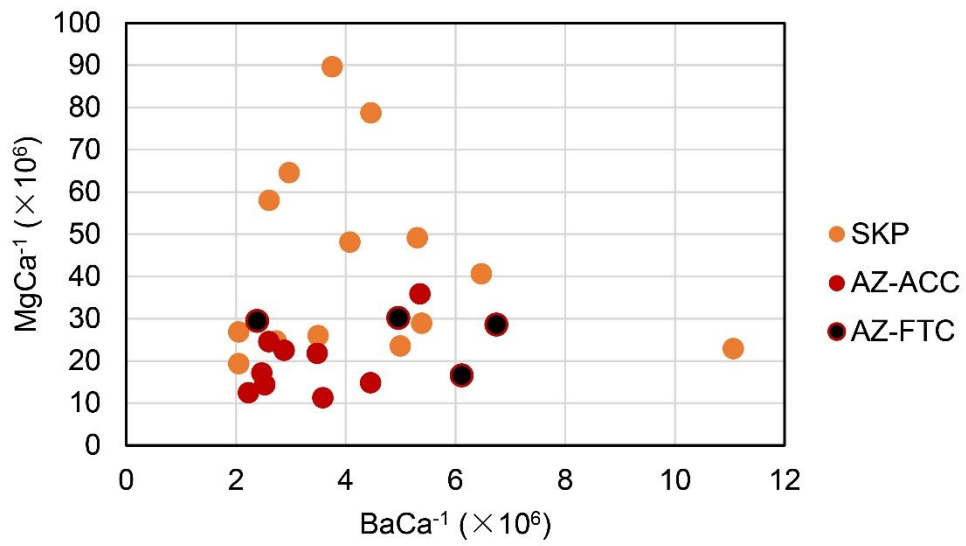
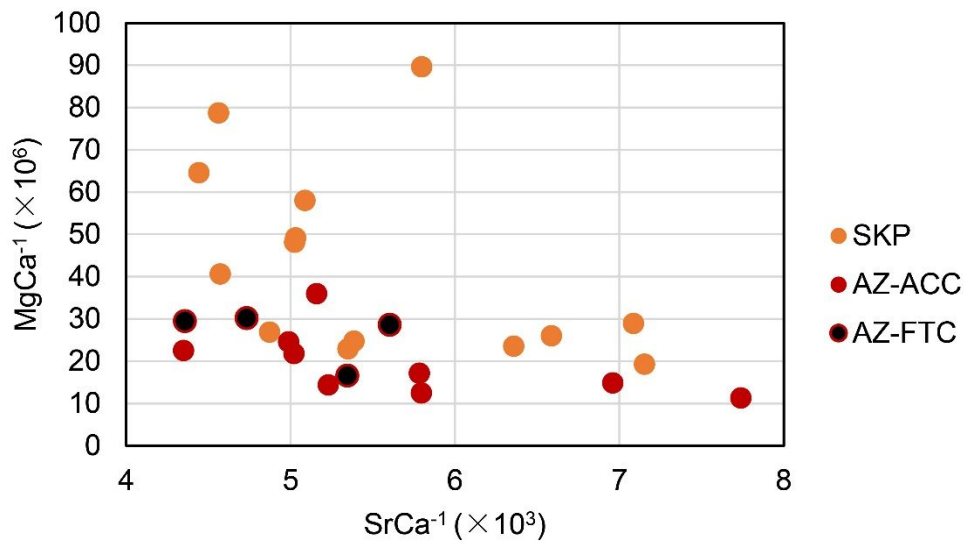
Figure 5. Otoliths of *E. antarctica* viewed under reflected light. Panels show the morphology of the a) sagittal otolith (whole otolith before sectioning), and b) transverse section of same otolith, showing translucent nucleus and spot rasters for laser ablation (red); 1: nucleus, 2: first translucent zone (age 0+), 3 – 4: translucent zones from age 1+ to age 2+, 5: edge of otolith transverse section (age 3+). Abbreviation is SL: standard length.

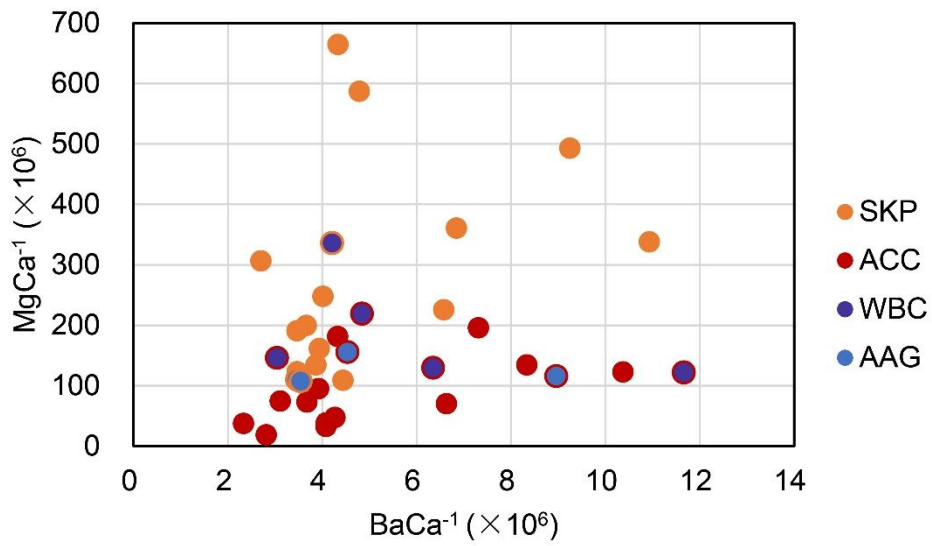
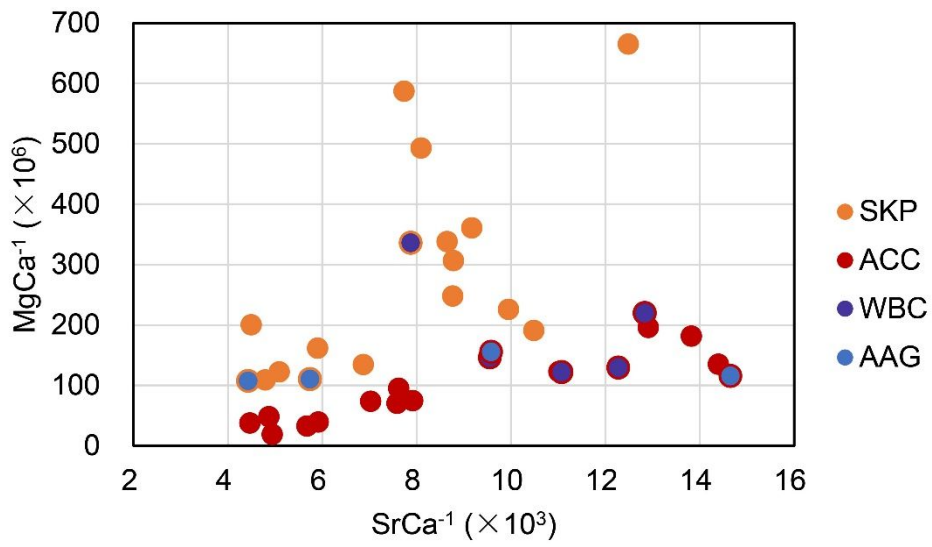
220x75mm (150 x 150 DPI)

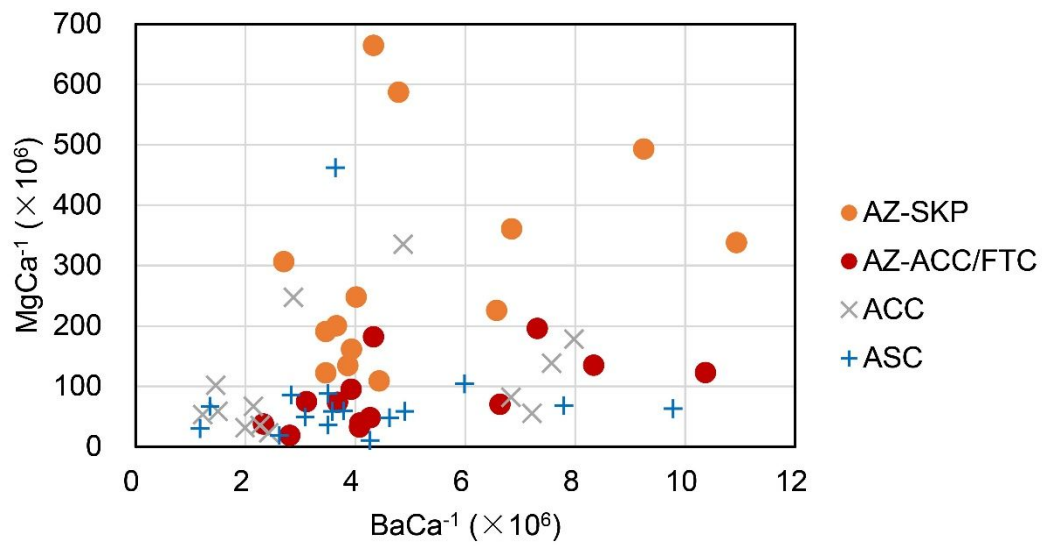
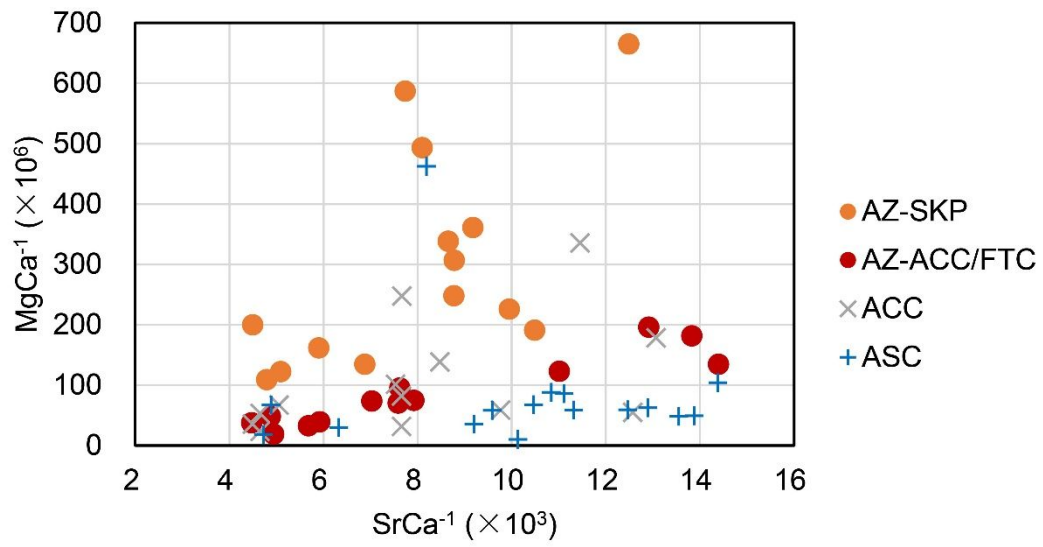
a)



b)







Supplementary materials

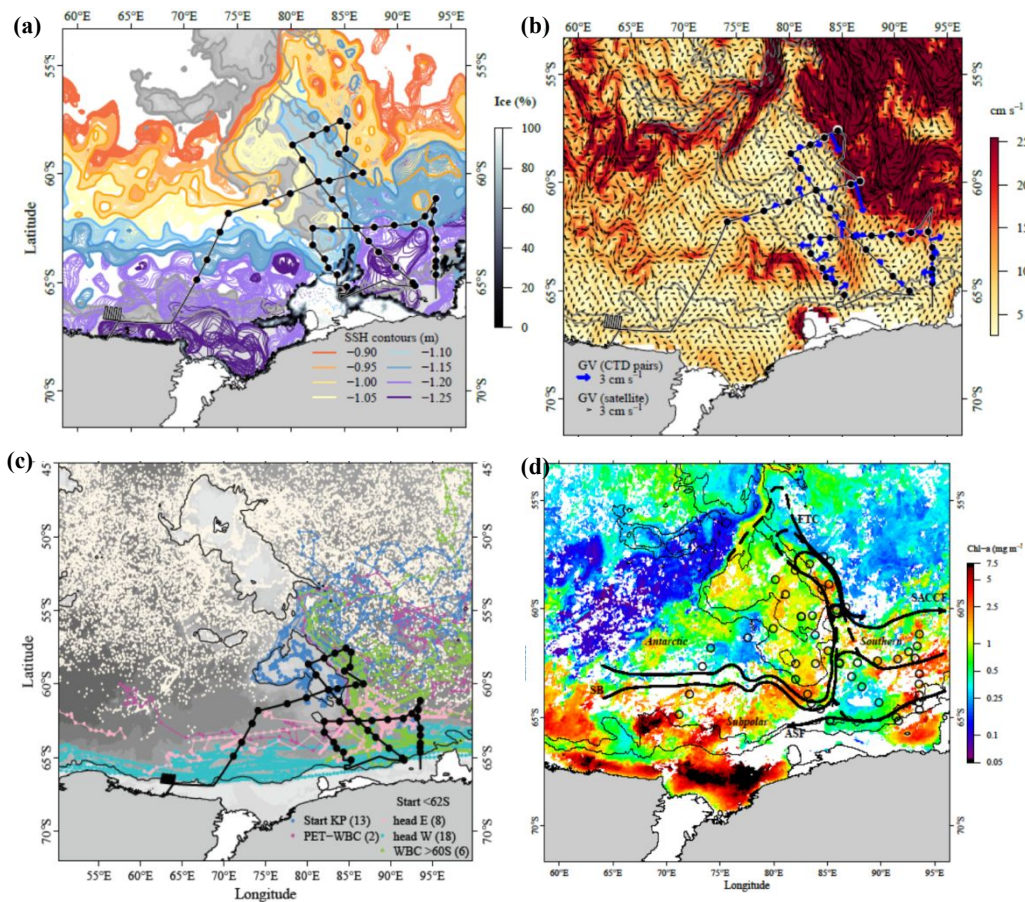


Figure S1. Regional ocean circulation and productivity over the southern Kerguelen Plateau during the Kerguelen Axis (K-AXIS) survey period 18 January - 18 February 2016, reproduced from Bestley et al. (2018, their Figures. 6a, b, 7b and 9). a) Daily absolute Sea Surface Height (SSH) streamlines (-0.95 m to -1.20 m) in relation to the cruise track (black); predominantly zonal flow is evident west of the southern Kerguelen Plateau (SKP), with streamlines demonstrating the topographic steering of flows northward and southward around the SKP. b) Maximum geostrophic velocities (GV) during the survey period, capped at 25 cm s^{-1} to highlight circulation features beyond the eddy-rich northeast domain. Vectors (black arrows) indicate the mean

current direction. c) Historical Argo float trajectories highlighting floats with southern (i.e., south of 62 ° S) origins. The blue floats (n = 13) of southern Kerguelen plateau origin are referred to in the text. Abbreviations are KP: Kerguelen Plateau; PET: Princess Elizabeth Trough; WBC: Western Boundary Current. d) Mean sea surface chlorophyll-*a*, noting the colour bar is on a natural log scale in mg m⁻³. Circulation features from Bestley et al. (2018) are as in Figure 2, main manuscript.

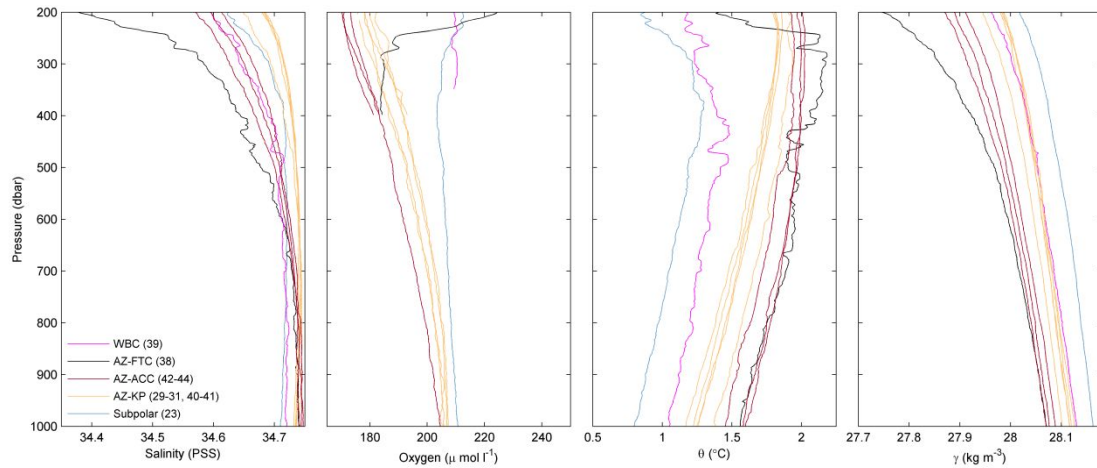


Figure S2. CTD profiles for MIDOC sample stations along T9 and T6. CTD: conductivity-temperature-depth; MIDOC: midwater opening/closing multiple cod-end device net. Abbreviations are WBC: Western Boundary Current. AZ-KP: Antarctic Zone corresponding to the Kerguelen Plateau; AZ-ACC: Antarctic Zone corresponding to the Antarctic Circumpolar Current; AZ-FTC: Antarctic Zone corresponding to the Fawn Trough Current. PSS: practical salinity scale.

Supplement text

As zonal flow approaches the Kerguelen Plateau, steering of the Southern Antarctic Circumpolar Current Front northern branch northward around BANZARE Bank and through Fawn Trough is evident from satellite-based dynamic height streamlines and geostrophic velocities (Supporting information Figures S1a and S1b). Quiescent water over the southern Kerguelen Plateau (SKP) is clear from six Argo floats that recorded residence times ranging between 421 - 1075 days, typically showing a slow anticyclonic drift (Supporting information Figure S1c). Moderate productivity over the SKP is evident from mean sea-surface Chlorophyll-a (Supporting information Figure S1d), which contrasts with low productivity in the Antarctic Circumpolar Current (ACC) waters in the Fawn Trough and north of the Northern branch of the Southern Antarctic Circumpolar Current Front.

The moderated ACC signature over the SKP compared to further west is shown by potential temperature-salinity curves along the zonal transect (T9) across the SKP (Figure 3, main manuscript), and vertical profiles at sampling stations (Supporting information Figure S2). The water properties at the Fawn Trough Current (FTC) station (Station 30 where midwater opening/closing [MIDOC] multiple cod-end device net was deployed) are notably different; here the subsurface properties indicate association with a meander of the southern Polar Front (Figure 3, main manuscript).

The vertical section along T9 (Figure 4, main manuscript) shows the ACC waters west of the plateau are characterized by very warm θ_{\max} waters (> 1.9 °C), extending over a broad range of salinity with the highest observed S_{\max} (> 34.74) and lowest oxygen values ($O_{2\min} \leq 175$ $\mu\text{mol l}^{-1}$) indicative of the oldest upper limb of the

Circumpolar Deep Water observed within the survey (Bestley et al. 2018). Shoaling isopycnals between 80°E – 82°E (CTD Stations 41 - 42) indicate a northerly flow (into the page) along the western flank of BANZARE Bank, whereas the strongly downward sloping isopycnals at 86°E (CTD Stations 38 - 39) are associated with the stronger southward flow (out of the page) of the FTC at the eastern plateau flank (Figure 4d, main manuscript). In contrast to predominantly zonal flow west of the SKP, satellite-based dynamic height streamlines (Supporting information Figure S1a) and geostrophic velocities (Supporting information Figure S1b) show complex mesoscale variability in the ACC east of the SKP, with extensive meandering of the fronts and both cyclonic and anticyclonic eddies.